

# Optical Trapping of Synthetic Diamond Particles Doped with Nitrogen Ions

HAMMAD ANWER



KTH School of Engineering Sciences  
Applied Physics Department

Master of Science Thesis  
KTH School of Engineering Sciences  
Applied Physics  
Stockholm, Sweden 2013

## ***Abstract***

Optical trapping (OT) is extensively used by physicists and biophysicists in order to study the mechanical properties of individual micron-sized particle and living cells, molecules. Over the last two decades, research approaches that link optical trapping with strong intensity of light have advanced the knowledge in this area of physics in a wide range.

While OT is purely suitable for trapping nano and micron-sized particles, various different techniques and trapping setups are pursued to secure highly focused light for better and stable trapping purposes. The goal of this study is mainly to design and to build a setup for OT to examine and to understand the behavior of nano-diamond particles doped with nitrogen ions. Besides the trapping of particles, a brief analysis of optical forces at different powers of light for characterization of the lateral and the axial movement of trapped particles has been done. Rayleigh optical trapping technique (single gradient beam trapping) is applied to trap  $100 \pm 5$  nm size nano-diamond particles by using a 1064 nm lasing system.

Besides performing the trapping of nano-sized diamond particles, the scanning of NV color centers in diamond is also performed in order to configure a trapping setup as a confocal microscope for characterization of many optical materials. Although the priority of the thesis project is the experimental details of designing and developing the setup for the OT, the same system has also an ability to work as a dual confocal microscope with different excitation lasing system.

## TABLE OF CONTENTS

---

Abstract	i
Acknowledgements	ii
Nomenclature	iii
Abbreviations	iv
List of Tables	v
List of Figures	vi
<b>1 Introduction</b>	<b>01</b>
1.1 Background	01
1.2 Diamond Defects as SPS	02
1.3 Application and Implementation of Optical Trapping	02
1.4 Objectives of the Research	02
<b>2 Optical Trapping</b>	<b>04</b>
2.1 Optical Forces	05
2.1.1 Scattering Force	05
2.2 OT Mechanism	08
2.2.1 Rayleigh Scattering Regime ( $r_p \ll \lambda$ )	08
2.2.2 Geometrical Optics Regime ( $r_p \gg \lambda$ )	10
2.3 Efficiency of OT	12
2.4 Types of Optical Trapping	12
2.4.1 Single Trap Setup	12
2.4.2 Multiple Trap Setups	14

2.4.3	Holography	14
<b>3</b>	<b>Characterization of Diamond, Its Defects and Surface Damages</b>	<b>16</b>
3.1	Properties of Diamond	16
3.2	Types of Diamond	17
3.2.1	Type I	17
3.2.2	Type II	18
3.3	Description of Diamond Synthesization	19
3.3.1	High Pressure and High Temperature	20
3.3.2	Chemical Vapour Deposition Method	20
3.3.3	Application of Polycrystalline and Single Crystalline Diamond	22
3.3.4	Damage and Defects of Diamond	22
<b>4</b>	<b>NV Colour Centers in Diamond</b>	<b>24</b>
4.1	NV Centers in Diamond	24
4.2	Atomic Arrangement in Crystal Structure	25
4.3	Phonons	27
4.4	Charge State of NV Centers in Diamond	28
4.5	Energy Level of NV Centers	30
4.6	Photo-chromic Effect of NV Centers	31
<b>5</b>	<b>Sample Preparation</b>	<b>34</b>

<b>6</b>	<b>Experimental Setup</b>	<b>36</b>
6.1	Confocal Microscope	36
6.1.1	Laser source	38
6.1.2	Mirrors	38
6.1.3	Pinhole	39
6.1.4	Objective	39
6.1.5	Filters	41
6.1.6	Detectors	41
6.1.7	Optical Fibers	41
6.2	HBT Setup	44
6.3	Spectrometer	45
6.4	CCD Camera	46
<b>7</b>	<b>Results and Future Work</b>	<b>47</b>
7.1	Testing the Microscope Setup	47
7.2	Scanning of NV Color Center	48
7.3	Scanning for Different Samples	49
7.4	Results of Optical Trapping	52
7.5	Future Work	55
7.5.1	NMR Imaging	55



## **Acknowledgements**

First of all, I would like to sincerely thank my supervisor, Prof. Mohamed Bourenane, for giving me the opportunity to work in a very interesting field of research, for guiding, and for supporting me. I would also like to thank my co – supervisor Alley Hameedi for his guidance and help in the lab when preparing the dual confocal microscope. Moreover, his demonstration for teaching me how to configure and testing the newly-built custom-designed dual confocal microscope was very helpful for me when working alone in Lab.

I would like to express my deepest and sincere appreciation to my supervisor for his support, guidance and for letting me do research in the fascinating world of the applied quantum and nano physics. In particular, a great deal of gratitude goes to all of the members of the KIKO group, especially my lab mates Elias Amselem, Muhammad Sadiq, Johan Ahrens, Alley Hameedi, Hatim Azzouz, Mohamed Nawareg, Ashraf Abdelrazig and Kate Blanchfield, as well as Ian Davidson and Jens Tellefsen who also has helped me with proof-reading the thesis.

Finally, I would like to thank my family for the love and support that they always provide. Most of all, my deepest and sincere gratitude goes to my elder brother Adeel, who is and will always be by my side!

## Nomenclature

$\vec{E}$	Electric Field.
$\vec{H}$	Magnetic Field.
$P_R$	Radiation Pressure.
$n$	Refractive Index.
$h$	Planck's Constant.
$\lambda$	Wavelength.
$\lambda_{exc}$	Excitation Wavelength.
$n_m$	Refractive Index of a Medium.
$n_p$	Refractive Index of a Particle.
$n_d$	Ratio between the Particle's and the Medium's Refractive Indexes.
$r_p$	Radius of Particle.
$F_{scat}$	Scattering Force.
$F_{grad}$	Gradient Force.
$F_T$	Total Force.
$\Delta\rho$	Change in the Momentum.
$I_o$	Intensity of Light.
$Q$	Trapping Quality Factor.
$P$	Power of Incident Light.
$w_o$	Beam Waist.
$n_g$	Refractive Index of Glass.
$n_{oil}$	Refractive Index of Oil.
$f$	Focal Length.
$\theta_i$	Angle of Incidence.
$\theta_r$	Angle of Reflection.
$\theta_c$	Critical Angle.



## List of Abbreviations

PDC	Parametric Down Conversion
HBT	Hanbury – Brown Twiss.
EMR	Electromagnetic Radiation.
OT	Optical Trapping
SLM	Spatial Light Modulator
DOEs	Diffraction Optical Elements
OTs	Optical Traps
HPHT	High Pressure and High Temperature.
CVD	Chemical Vapour Deposition.
CBN	Carbon Boron Nitride.
EPR	Electron Paramagnetic Resonance.
IR	Infrared Radiation.
UV	Ultraviolet Radiation.
ZPL	Zero Phonon Line.
TDBC	Tetrachlorobenzimidazolocarboyanine.
NA	Numerical Aperture.
MAG	Magnification.
CdSe	Cadmium Selenide.
NMR	Nuclear Magnetic Resonance.
QDs	Quantum Dots.
FCC	Face-Centred Cubic
BCC	Body-Centred Cubic
APDs	Avalanche Photo Diodes
Nd:YAG	Neodymium-Doped Yttrium Aluminum Garnet
SPS	Single Photon Source

## List of Tables

Table 1: Values of universal and physical constants of diamond.	17
Table 2: Levels of impurities in different diamond categories and manifestation forms of diamonds.	18
Table 3: Different defect centers in different types of diamond.	23
Table 4: ZPL wavelengths and associated zero phonon energy of two charge-states of nitrogen vacancy centers in diamond.	28
Table 5: Calculated value of lateral, axial and confocal resolution of confocal microscope for the 532 nm and the 687 nm excitation laser system.	38
Table 6: Number of modes propagating along the MMF and SMF with different values of core diameter.	42
Table 7: Calculated values of the beam waist, the radius and the trapping volume of the laser.	53

## List of Figures

- Figure 2.1: Schematic diagram of momentum transfer from a focused TEM<sub>00</sub> Gaussian beam to a spherical particle positioned in the beam waist. 09
- Figure 2.2: Illustration of the Mie particle movement in the lateral direction with different rays of light and intensity. 10
- Figure 2.3: Illustration of the Mie particle movement in the axial direction with different rays of light focused at different points. 11
- Figure 2.4: A typical setup of an inverted microscope to trap the particle at FFP while using the 1064 nm lasing system. 13
- Figure 4.1 Structure of a unit cell for (a) simple cubic lattice structure, (b) body centred cubic, lattice structure and (c) face centred cubic lattice structure. 26
- Figure 4.2: (a) Structure of the diamond unit cell with chemical bonds drawn between two nearest neighbour's atoms. (b) Diamond lattice structure after a rotation of 30 in the x axis and 60 in the y axis direction. 27
- Figure 4.3: (a) Structure of the nitrogen – vacancy centre in diamond, where nitrogen atom is shown in brown, nearest carbon atom to the vacancy shown in green colour and the vacancy is shown in white colour with a bonding with carbon atom. 29
- Figure 4.4: Traces of the spectrometer for each individual NV charge state. 29
- Figure 4.5: The energy level diagrams of NV centres. (a) The 3 – level structure of NV<sup>-</sup> centre showing a bunching effect at high excitation power.(b) The 2 – level structure of NV<sup>o</sup> color centre which is suitable for obtaining perfect antibunching curve at both high and low excitation power. 30

- Figure 4.6: The diagram showing the energy level of nitrogen color center consisting of  $^3G$  grounds and the excited  $^3A$  state. 31
- Figure 5.1: Representing the basic idea of sample preparation and the prepared sample itself. The image 5.1(a) consists of the schematic diagram of the optical tweezer sample and image 5.2 (b) shows the real sample. 35
- Figure 6.1: The schematic diagram of a dual confocal microscope used for imaging the defects in diamond, QDs of CdSe, and TDBC molecules. This setup is also used for OT of diamond particle doped with nitrogen. 37
- Figure 6.2: The diagrammatic representation of the difference between the MMF and SMF fiber for propagation of laser light from core of the fiber. 44
- Figure 6.3: The picture showing the structural diagram of a multimode fiber (MMF) and a single-mode fiber (SMF). Orange and yellow color represent the protective plastic skins of MMF and SMF. 44
- Figure 6.4: The schematic diagram of the HBT setup used to calculate the value of the second-order correlation function, showing the start and stop values for  $g^2(\tau)$  function for drawing the antibunching curve. 45
- Figure 7.1: The image of a diffraction grating at a widened field illumination is taken with a CCD camera. 47
- Figure 7.2: The figure showing the results of the confocal microscope scanning. The images (a) and (b) shows the different portions of the diffraction grating pattern scanned with different values of the focus points using  $2 \mu\text{W}$  of pump laser. 48
- Figure 7.3: Results of broad-area scanning of the NV centers in diamond. (a) Image of a few NV centers obtained during broad-area scanning of  $200 \times 200 \mu\text{m}^2$ . (b) Image of single NV centers in diamond particles obtained during a fine area scanning of  $10 \times 10 \mu\text{m}^2$ . 49

- Figure 7.4: Scanning resultants of QD (CdSe) samples in broad-area scanning of  $80 \times 80 \mu\text{m}^2$  and a fine-area scanning of  $30 \times 30 \mu\text{m}^2$ . 50
- Figure 7.5: The scanning results of the dual microscope setup by using the 687 nm laser. 51  
 (a) Image of a broad-scanning of the sample in a  $200 \times 200 \mu\text{m}^2$  area. (b) The image of fine scanning of the sample in a  $2 \times 2 \mu\text{m}^2$  area with different values of the focus.
- Figure 7.6: The schematic diagram of trapped and suspended diamond particles in the beam waist. 52
- Figure 7.7: The captured images of manually moving the suspended diamond particles in the X, Y axes towards the focus of the 532 nm laser on the sample. 53  
 Image 7.7 (a) the diamond particle is moving to the right along the x – axis towards the focus point and in the image of 7.7 (b) the diamond particle is moving upwards along the Y – axis towards the focus point.
- Figure 7.8: The captured images of the trapped and suspended diamond particles at the focus of the 532 nm and 1.064  $\mu\text{m}$  laser upon the sample. 54  
 Images 7.8 (a) and (d) show the diamond particle moving along the X – axis. Images 7.8 (b) and (c) show when the diamond particle is moving to the upward along Y – axis.

## **1.1 Background**

The quantization of electromagnetic energy was first proposed by Max Planck in 1900 by postulating and hypothesizing that the energy of a harmonic oscillator is quantized. Later in 1905, the basic idea of the photon was central to the explanation of Einstein's idea of the photoelectric effect. This early work of Planck and Einstein was pivotal in the development of the quantum theory of light [1]. The development of the laser since (coherent light source) has been very rapid and in fifty some years after the invention of the laser, the applications of laser light have amazingly recast the life of mankind [2, 3].

In addition to the many domestic levels of applications, lasers have also numerous ranges of industrial level applications such as cutting and welding, remote sensing, surveying, weapon systems, communication, printing and medicine. Besides these astonishing applications, the laser also has the ability to physically manipulate the microscopic structure of matter [4, 5].

The development of optical trapping techniques was pioneered in the early experiments where the microscopic structures were pushed by a radiation pressure. The idea of optical trapping was first reported by A. Ashkin in 1969 [3], who demonstrated trapping of dielectric particles in the size range of 20 nm - 10  $\mu$ m. Ashkin based his technique upon the balance of radiation forces such as scattering force and the gradient force in order to trap the particles. In the year 1971, while working in Bell Labs, Ashkin and his colleagues were performing a successful experimental demonstration of optical trapping of dielectric particles [5, 6].

In 1997 an American physicist, Steven Chu earned the Noble Prize in physics for trapping particles while using the same technique as Ashkin for trapping neutral particles having diameter sizes larger than 100 nm [6].

## ***1.2 Diamond Defects as SPS***

The intrinsic defects in natural diamond and the extrinsic defects in synthetic diamond are good sources of fabricating a single-photon source (SPS). SPSs are quite different from the classical sources of light because on average, SPSs only emit one photon at a regular interval of time. In recent years, stable and efficient single-photon emission has been examined in a wide range of sources, including single molecules, single atoms, trapped ions, quantum dots, color centers in crystals, color centers in diamond and in spontaneous parametric down conversion (SPDC).

Single photons are highly important when it comes to the understanding of the fundamental nature of light because single-photon states disclose a number of properties which otherwise cannot be interpreted by classical theories.

## ***1.3 Application and Implementation of Optical Trapping***

Difficult technical and nonlinear optical effects are required in order to perform optical trapping of single individual diamond particle suspended in liquids. The setup for optical trapping ranges from the simple-lens based setup to the complex integration of different lens-based setups with multi-laser beams. OT is an important tool for manipulating the microscopic object through confinement, organizing atomic arrangements, assembling of particular structures along with the modification of microscopic objects. OT setups are also useful for the study of biological objects such as viruses, the movement of bacteria, living cells and for the study of mechanical mechanism of DNA beads. The applications of optical trapping are therefore interconnected between atomic physics and the medical sciences [9, 10].

## ***1.4 Objectives of the Research***

The objective of the research reported in this thesis is the optical trapping of spherically shaped diamond particles suspended in liquids at room temperature. These diamond particles are doped with nitrogen ions to create color centers in the diamond lattice. The color centers in the diamond structure especially nitrogen atoms, are also an ideal source for single-photon emission

[11, 12]. The optical trapping of nitrogen doped diamond particles is performed with a cw 1064 nm laser system while a cw 532 nm laser is used to excite the NV color centers in the particles.

Besides the above mentioned project targets, my master thesis also deals with the custom designed and the preparation of a dual confocal microscope. This newly custom-built setup is used to characterize the different samples along with the optical behavior of nitrogen vacancy center in diamond. The results expected from this new setup are more efficiently obtained than that of the photons obtained with the earlier designs. The expected results also depend upon the sample preparation technique and the number of nitrogen vacancy centers in nano-diamonds. Specially created software is also used to control the piezo-system and to built-up the scanning image of the specimens while running the setup for scanning the sample.



## 2 OPTICAL TRAPPING

---

Light is a form of energy quanta carrying not only the energy but also the momentum of the light, it can also exert the force on material bodies by transferring of momentum as was proposed by Johannes Kepler. However, after the pioneering work of J. Kepler [12, 13], it took a long time for James Clerk Maxwell to explain optical trapping phenomena theoretically [13]. In 1901, Pyotr Lebedev performed a successful experimental demonstration of optical forces that acting on material objects, can significantly strengthen theoretical explanation Maxwell ideas [14].

Light as an electromagnetic field travelling in a specific direction carries both energy and momentum. The energy transferred by an electromagnetic field to a material object in a certain time is defined by the Poynting vector;

$$\vec{S} = \frac{c}{4\pi} \vec{E} \times \vec{H} \quad (2.1)$$

Where  $c$ ,  $H$ , and  $E$  are the speed of light, the magnetic and electric fields respectively. If  $\langle \vec{S} \rangle$  is considered as a time average value of energy transferred than the radiation pressure on the objects is given by,

$$P_R = \frac{\langle S \rangle}{c} (1+r) n \quad (2.2)$$

Here,  $n$  represents the refractive index of the medium and the value of  $r$  is chosen between  $r = 0$  for black bodies and  $r = 1$  for perfectly reflecting surfaces and latter shows the reflectivity of the medium under radiation pressure [15].

In the 1930s, the development of quantum mechanics produced the explanation of radiation pressure from a quantum prospective. Light can now be thought of as being composed of small particles known as photons where each photon carrying energy of  $E = h\nu$  and a momentum  $P$ , defined by de Broglie relation i.e.

$$P = \frac{h}{\lambda} \quad (2.3)$$

The phenomenon of optical trapping was very difficult to demonstrate with thermal or classical light sources due to the variation in the light intensity 'I'. In the 1960s, after the invention of the laser, the experimental demonstration of OT was possible with coherent light. In the 1970s, a decade later, A. Ashkin performed a successful experiment for trapping of dielectric particles by using a ultra-violet coherent light source. Because a laser can have a very high intensity which could easily be focused on a small object to transfer the sufficient amount of energy and momentum and these experiments were very successful [3, 16].

The mechanism for the photons energy and momentum transferred to an object leads to an exerted optical force on the object in the direction of the photons propagation. The basics of the OT forces acting on an object can completely be interpreted by observing the intensity, the momentum, and the direction of propagation of light as it is changed after the interaction with the object.

## ***2.1 Optical Forces***

These optical forces are based upon the interaction of the light with very small objects placed in the path of light the beam. The magnitude of these optical forces is in the nano and the pico newton scale.

### ***2.1.1 Scattering Force***

The generation of the scattering force in OT originating from the surface of a particle is totally dependent upon the phenomena of scattering of light from the particle. When a photon flux is scattered from a particle, the two components of the scattering force emerges, one is in the direction of light propagation and the other in the opposite direction of the scattering phenomena. Scattering forces act in the opposite direction of the scattered photons. Scattering forces of the photons depend upon the intensity of the focused light because its acts along the direction of propagation of the light.

The total scattering force for an OT is thus calculated as the total change in the momentum of the photon before and after the scattering event, and can be expressed as follows:

$$F_{Scat} = \frac{n}{c} \iint (s_{in} - s_{out}) dA$$

$$= \frac{n_m \sigma \langle S \rangle}{c} \quad (2.4)$$

Here  $\langle S \rangle$  is the Poynting vector and  $\sigma$  is the Rayleigh scattering cross-section for a spherical particle. It can be written as [20].

$$\sigma = \frac{8}{3} \pi \left[ \frac{2\pi n_m}{\lambda} \right]^4 r_p^6 \left[ \frac{n_d^2 - 1}{n_d^2 + 2} \right]^2 \quad (2.5)$$

So, after inserting the value of  $\sigma$  in to equation 2.4, it will become,

$$F_{Scat} = \frac{128\pi^5 r_p^6}{3\lambda^4} \left[ \frac{n_d^2 - 1}{n_d^2 + 2} \right]^2 \frac{n_m I_o}{c} \quad (2.6)$$

Here,  $n_d$  is the ratio of the refractive indices of the particle  $n_p$  and the medium  $n_m$ . The factor  $r_p$  is the value of the particle radius for Rayleigh particle ( $r_p \ll \lambda$ ). Thus from equation (2.6), the value of the scattering force is dependent on the wavelength of the trapping laser, the size of the particle and the intensity of the photon flux [16 ,20].

### 2.1.2 Gradient Force

The interaction of light with a particle in the vicinity of the beam waist produces a gradient force on the particle due to the particles dielectric response. Thus the interaction of the beam electric field with the induced dipole establishes an electrostatic potential which define as:

$$U = -p \cdot E \quad (2.7)$$

Thus, the gradient force due to the spatially varying intensity of the light field is given as:

$$F_{grad} = -\nabla U$$

$$= -p \cdot \nabla E \quad (2.8)$$

Here  $p = \alpha E$  is the induced dipole moment of the continuous electric field of the atoms, which gives us the following expression:

$$F_{grad} = -\alpha(\nabla \cdot E)E \quad (2.9)$$

So, for a Rayleigh particle ( $r_p \ll \lambda$ ), the gradient force for the OT of small particles with radius  $r_p$  is obtained from equation (2.9) as:

$$F_{grad} = -\frac{n_m^3 r_p^3}{2} \left[ \frac{n_d^2 - 1}{n_d^2 + 2} \right] \nabla E^2 \quad (2.10)$$

Here as before,  $n_d = n_p / n_m$  is the ratio between the refractive index of the particle and the surrounding medium. Thus from equation (2.10), the value of the gradient force is dependent upon the radius of the particle and the electric field intensity. The gradient force acts as an attractive force for a particle in the beams vicinity. If  $n_p \gg n_m$ , then the trapped particle is pulled towards the higher electric field intensities. While on the other hand, if  $n_p \ll n_m$ , then the trapped particle will be pushed away from the high electric field. (This means that the value of the scattering force is much greater than the value of the gradient force, so the particle is gradually pushed away from the beam waist). The following are the important condition for selecting the particles and medium for effective OT:

- i. For dielectric particles, the value of the refractive index of the particle and that of the surrounding material play key roles in achieving stable OT. A particle of size 25 – 30  $\mu\text{m}$  can be easily trapped using the attractive gradient force. OT of larger particles (particle size range larger than 25 – 30  $\mu\text{m}$ ) is not possible by applying the optical force with high NA objective, because the value of the gravitational force greater is than both the scattering and the gradient force value [20].
- ii. For the Rayleigh OT regime with particle radius ( $r_p \ll \lambda$ ), in the case of a metallic particle which size range of 40 – 50 nm in diameter, they can be easily trapped with the single-beam trapping mechanism. Particles in this size range can easily produce strong gradient forces due to the high polarizability needed for balancing the scattering forces.

Thus metallic particles sized in micrometer and dielectric particles of size  $> 30 \mu\text{m}$ , with refractive index values of  $n_p \ll n_m$  cannot be trapped with a single beam [15, 16, and 20].

## **2.2 OT Mechanisms**

The working of an OT setup is based upon the balancing of the optical forces arising from the microscopic particle interacting with light. These optical forces can be resolved into two different forces and the magnitude of each of these forces depends upon the reflectivity of the trapping medium. When an object (dielectric particle) is positioned around the beam waist (where the intensity of the light is very high and all of the energy and the momentum of the photons are focused), then the light will be reflected, refracted or even absorbed by the particle. Thus, the processes of reflection, refraction and absorption give rise to the generation of two optical forces and the observations of these forces reveal the secrets of OT with highly focused light. The size of the focused beam waist at the front focal plane (FFP) of the objective is of  $\mu\text{m}$  scale.

The optical forces arising from the interaction of the dielectric particle with the light is given by the change in total momentum flux ' $\rho$ ' of the beam at the FFP,  $F = \Delta\rho$  [14]. So, the total change in momentum ' $\Delta\rho$ ' of the photon flux is balanced by an equal and opposite change in the momentum of the particle in the direction of the propagation of the light. The total change in momentum ' $\Delta\rho$ ' of the photon flux is also the reason for the optical forces according to the Newton's law;

$$\vec{F} = \frac{d(\Delta\rho)}{dt} \quad (2.11)$$

### **2.2.1 Rayleigh Scattering Regime ( $r_p \ll \lambda$ )**

In the Rayleigh scattering regime, the radius of the spherical particle is much smaller than the trapping wavelength of the light. Thus the particle will act as a single dipole which will split the optical forces into two components. The scattering force that emerges from the dipole acting

upon the absorption and the re – radiation of the light in the direction of the incident light, can be written as:

$$F_{Scat} = \frac{128\pi^5 r_p^6}{3\lambda^4} \left[ \frac{n_d^2 - 1}{n_d^2 + 2} \right]^2 \frac{n_m I_o}{c} \quad (2.12)$$

The other component of the optical force is the gradient force which is controlled by the intensity gradient of the a focused beam onto the spherical particle and is given by;

$$F_{grad} = -\frac{n_m^3 r_p^3}{2} \left[ \frac{n_d^2 - 1}{n_d^2 + 2} \right] \nabla E^2 \quad (2.13)$$

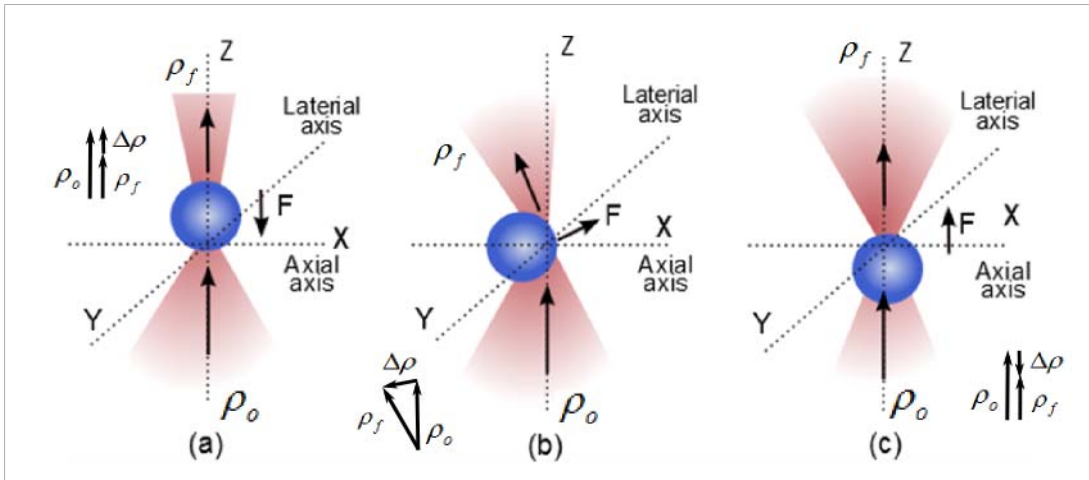


Figure 2.1: Schematic diagram of momentum transfer from a focused TEM<sub>00</sub> Gaussian beam to a spherical particle positioned in the beam waist [16].

The intensity gradient of the incident light is controlled by the power of the incident light. The magnitude and the direction of these two optical forces play an important role for achieving stable OT with a single beam. The direction of  $F_{scat}$  and  $F_{grad}$  must be in opposite direction so as to accomplish stable axial trapping of the particle. The magnitude of  $F_{grad}$  is greater than that of the  $F_{scat}$  and the value of the ratio between them,  $F_{grad} / F_{scat}$  must be greater than unity, since  $F_{grad}$  is acting against the combination of gravitational force and  $F_{scat}$  for stable OT.

Figure (2.1) shows the momentum transferred from a focused TEM<sub>00</sub> Gaussian beam to a spherical particle situated at the beam waist of size  $w_0 = \frac{n\lambda}{\pi NA}$ . In figure 2.1(b), the particle moves to the right because the optical forces are acting on it from the right and the transfer of the momentum from the particle in the left direction due to the refracting property of the light. But, in figure 2.1(a) and (c), is shown that the movement of the particle can also be controlled in the axial direction by the transferring of momentum at different points of focus. The direction of the total optical forces is in the opposite direction to the beams propagation direction. Since, when a beam is focused away from the central point of the particle, the particle will move into the beam. The net optical forces are acting in the downward direction in which case the particle motion is against the direction of propagation of the light. But the situation is opposite for the particle movement with direction of propagation of light.

### 2.2.2 Geometrical Optics Regime ( $r_p \gg \lambda$ )

In the geometrical optical regime (also known as the Mie regime), OT is independent of the trapping wavelength of the light and ray optics techniques are therefore used to forecast the optical forces for a scattering particle with larger radius.

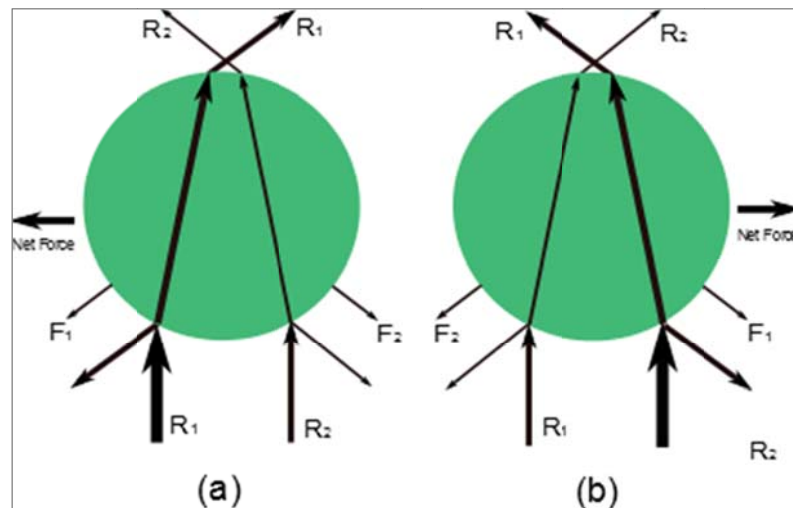
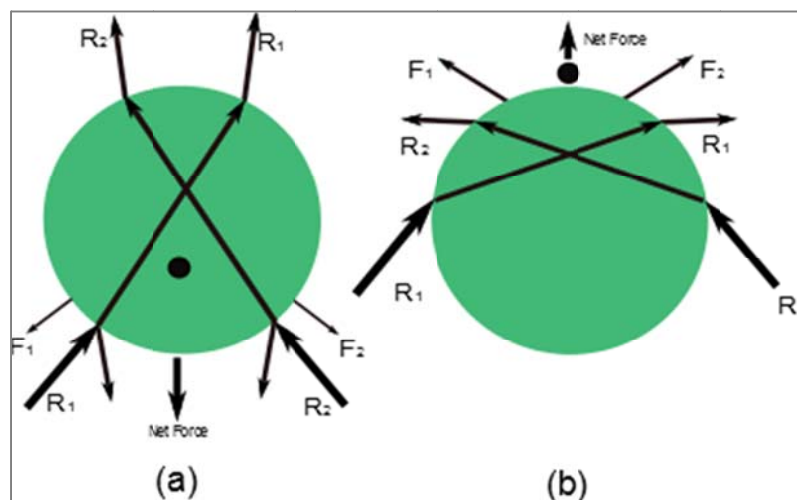


Figure 2.2: Illustration of the Mie particle movement in the lateral direction with different rays of light and intensity [18]

For a stable OT to occur in the geometrical optical regime, it is accomplished by a single force. This single optical force is ensued from a combination of  $F_{grad}$  and  $F_{scat}$  from a large particle with a high refractive index value. A large particle in the geometrical optical regime, with radius  $r_p \gg \lambda$ , acts as a small positive lens to reflect and refract the rays. A technique of multi – ray trapping is used to trap the larger particles in the Mie regime. Figure (2.2) illustrates the technique used for trapping with a laser beam with different intensity focused on the Mie particle to move the particle in the lateral direction.

In figure 2.2 (a), the net optical force as applied to the Mie particle is in the left direction where the intensity of the trapping laser ray ‘  $R_1$  ’ has high intensity as compare to ray  $R_2$ , so the particle moves in the direction of the high intensity which means moving left. But in figure 2.2 (b), the Mie particle moves in the right direction, because of the reaction of all of the optical forces (  $F_{grad}$  and  $F_{scat}$  ), applied in the right direction where the intensity of trapping laser is very high.



**Figure 2.3:** Illustration of the Mie particle movement in the axial direction with different rays of light focused at different point [18, 19].

Figure 2.3 shows the axial trapping movement of the same particle into the direction of the trapping laser with different incoming rays. In figure 2.3(a), the black spot on the surface of the Mie particle represents the focal point of the trapping laser. If the focus of the laser is moved away from the actual focal point, the collective reaction of the optical forces from different rays on to the particle moves the particle towards the focused point which causes the particle to move in the opposite direction to the trapping laser. In the second case, the real focal point of the



trapping laser is moved away. This situation is displayed in figure 2.3(b) situation. The reaction to the optical forces is different in this condition since all of the forces collectively push the Mie particle towards the focal point and into the direction of the propagation of the trapping laser.

### **2.3 Efficiency of OT**

The efficiency of the OT setup depends upon the quality factor ‘Q’ and the values of this factor relate to the physical specifications of the setup. This quality factor is a dimensionless quantity which expresses the process of converting the incident power of light into the optical forces [20]. In order to calculate the value of the quality factor Q for an optical setup, the total force acting on a particle is given by vector sum of  $\vec{F}_{scat}$  and  $\vec{F}_{grad}$ .

$$\begin{aligned}\vec{F}_{Tot} &= \vec{F}_{grad} + \vec{F}_{scat} \\ &= Q \frac{n_m P}{c}\end{aligned}\tag{2.13}$$

Here  $n_m$  is the refractive index of the surrounding material and P is the power of the incident light at the back focal plane of the objective. The maximum value of ‘ $F_{Tot}$ ’ is dependent upon the value of the refractive index of the medium, the intensity of the incident light and the maximum value of Q which in turn, relates to the NA of the objective lens, the wavelength of the trapping light, the mode and the polarization state of the light, the ratio of the refractive index  $n_d$ , the size and shape of the trapped particle [21].

## **2.4 Types of Optical Trapping**

### **2.4.1 Single Trap Setup**

The trapping of particles is performed with an optical setup built with high NA objective in the form of an inverted microscope. The purpose of using a high NA objective is to focus more light at the FFP of the objective in order to position the trapped particle at the center of the field of view of the microscope [16]. The wavelength of the lasing system used for trapping in my setup

is 1064 nm. There are two main reasons for using this infra-red lasing system for trapping the particles:

- i. In the infra-red region the corresponding photons have not enough energy to produce any physical damage upon the interaction with the solids.
- ii. Another reason for using the 1064 nm wavelength is to minimize entrapping effect due high oscillation per second.

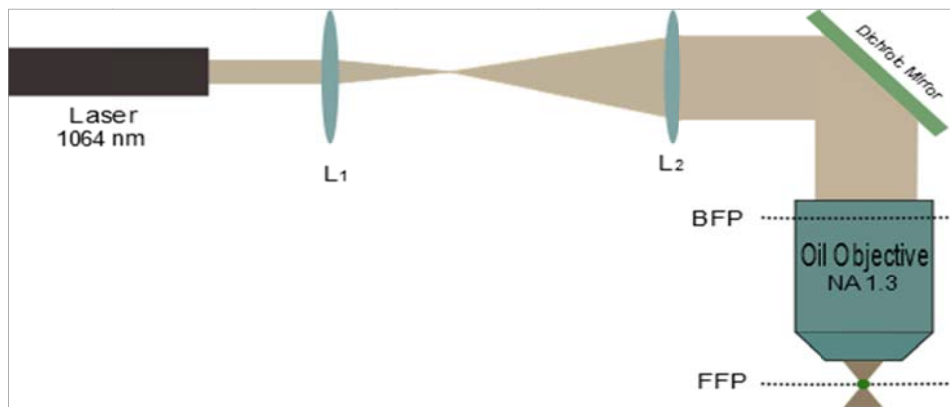


Figure 2.4: A typical setup of an inverted microscope to trap the particle at FFP while using the 1064 nm lasing system [16, 19].

Figure (2.4) shows a typical schematic diagram of an OT setup. The beam from the 1064 nm laser YAG is directed toward the BFP of the objective after being reflected from the dichroic mirror. This dichroic mirror has the ability to reflect the infra-red spectral region and transmit the visible spectrum with a high transmission factor. Lenses  $L_1$  and  $L_2$  in the setup are acting as a beam expander to overfill the BFP of the microscope objective so as to focus more light at the FFP.

The movement of the trapped particle in the lateral direction is controlled by the angle of incidence of the trapping beam at BFP of the microscope objective. The angle of incidence of the

beam is changed with the help of a gimbal mounted mirror<sup>1</sup> in order to maintain the same optical axis for the trapping setup.

### **2.4.2 Multiple Trap Setups**

The multiple trap setups are used to control each individual trapped particle by using different wavelengths of light recombined at the same optical axis of the BFP objective after separating and recombining the orthogonal polarization direction of the beam with the help of beam steering optics. The recombination of orthogonal polarization direction of the beam can also be performed with acousto optical deflector so that the beam can be centered at the center point of the BFP [16, 22].

A large number of particles can be trapped with a single beam and a larger particle can also easily be trapped with this technique after adjusting the angle of incidence at the BFP. But these trapped particles are restricted move only to in the single plane of trapping [22, 23].

### **2.4.3 Holography**

A multiple OT could be generated with a single beam by placing a diffractive optical element (DOE) in the path of the beam. Holography is a kind of multiple three dimensional OT and is a computer controlled trapping technique used for trapping the particle in a sample while using a single beam.

The OT performed with a spatial light modulator (SLM) based setup can be employed for DOE trapping, and the phase modulation of the SLM can be controlled by a computer. The arrangement and the movement of the OTs can now be controlled with the SLM because the position and movement of the OTs calculated by series of phase patterns. When these phase patterns are transferred to the SLM in a sequence then it will distribute the needed intensity of the light for the movement of the OTs an in specific direction. The setup we used as a single-trap

---

<sup>1</sup> For more information about the gimbal mounted mirror please visit thorlabs website. [www.thorlabs.com](http://www.thorlabs.com)

setup can be modified into a holographic optical trap setup after placing the SLM into the present setup.

### **3 CHARACTERIZATIONS OF DIAMOND, ITS DEFECTS AND SURFACE DAMAGES**

---

Entity of natural diamond has been known to mankind for over two thousand years. Diamond is a form of carbon allotrope, where each atom of carbon is arranged in an invariance of the FCC crystal structure that is defined as a diamond lattice. The FCC structure form of an atomic arrangement results in a strong covalent bonding between its atoms, which is the basic reason for its extreme hardness and ultra-incompressibility [23, 28]. The band-gap energy of diamond is 5.5 eV which corresponds to the deep ultraviolet. Pure and defects-free form of diamond appears as colorless under exposure to visible light.

The presence of color centers or defects, such as dislocations, vacancies and complexes in the diamond lattice will cause it to appear as a colored object used for creating electronic energy levels within the diamonds band-gap [25, 28]. Therefore, luminescence of different wavelengths appears from the specific energy structures of each of the defects and impurities in the material.

Naturally occurring diamonds are relatively rare. Diamond-related research is progressing in universities, laboratories, and in industries throughout the world to find new ways to meet the increasing demand of diamond for research purposes along with its commercial use. Thus, new techniques have been developed for the development of synthetic diamond in many laboratories around the world that can increase the growth of diamonds for potential use of the material in electronics, material science, medical area and quantum optics & quantum photonics [26, 29].

#### ***3.1 Properties of Diamond***

A diamond crystal consists of a tetrahedral arrangement of carbon atoms covalently bonded with  $sp^3$  hybrid bonds in the FCC form of lattice structure [28, 29]. Synthetic diamonds have distinct and important properties that make them a favorable material for advanced research and applications in quantum information processing. There are two main reasons for the unusual behavior of diamond:

- 1) Carbon atoms are small and very light, having a short-range  $sp^3$  bonds in the form of diamond structure.
- 2) The binding between two carbon atoms depends on very strong covalent bonds the in diamond structure, which is a reason for diamond hardness.

The table below outlines some properties and universal constants of diamond;

Table 1: Values of universal and physical constants of diamond.

Property	Value	Property	Value
Hardness	2 MPa	Dielectric strength	$1 \times 10^7$ V/cm
Strength/Tensile	90 – 225 GPa	Electron mobility	$2200 \text{ cm}^2/\text{V-s}$
Sound velocity	$1.8 \times 10^4$ m/s	Hole mobility	$1600 \text{ cm}^2/\text{V-s}$
Density	$3.53 \text{ g/cm}^3$	Bandgap	5.45 eV
Loss tangent at 40Hz	$6 \times 10^{-4}$	Resistivity	$10^{13} - 10^{16} \Omega \text{ cm}$
Young's modulus	1.22		
Poisson's ratio	0.2		
Thermal expansion coefficient	$1.1 \times 10^{-6} \text{ K}^{-1}$		
Thermal conductivity	20 W/cm – K		
Debye temperature	2200 K		
Refractive index	2.41 (591nm)		
Optical transparency	2.25		
Dielectric constant	5.7		

### 3.2 Types of Diamond

The diamond crystal can mainly be categorized into two major classes: type I and type II. Each of these two classes is further divided into two different subcategories such as types Ia, Ib, and types IIa, IIb [30]. The categorization of the two diamond classes depends upon the amount of the presence and the form of incorporated impurities such as nitrogen, silicon, nickel and boron in the diamond structure at atomic scale.

#### 3.2.1 Type I

Type I diamond is the most common form of diamond. Nitrogen atoms are the main impurity in this crystal structure. This type of diamond has the ability to absorb light in the infrared and the ultraviolet regions with the capability of shifting the absorbed wavelengths into longer wavelengths during the re – emitting process.

##### a) Type Ia

In the type Ia diamond, nitrogen atoms are present in the form of clusters within the diamond lattice. This is one type of natural diamond containing 0.1 – 0.3% of nitrogen impurity. Almost

98% of natural diamond belongs to this class. This diamond form usually absorbs blue light and will appear either a brown or a yellow color [31].





**b) Type Ib**

Type Ib diamonds are of high-pressure and high-temperature (HPHT) synthetic diamond class. These diamonds contain 0.05% of nitrogen impurity and the impurities are perfectly diffused and dispersed throughout the crystal structure. Type Ib diamond has a capability to absorb blue and green light. The appearance of this class of diamonds is darker than that of the type Ia diamonds due to the precise concentration and location of the nitrogen atoms in the crystal structure. This type of diamond is very rare in nature [35, 37, and 38].

**3.2.2 Type II**

Type II diamonds have no measurable scale for the amount of impurity, but they also contain some nitrogen atoms. The shape of the crystals has no symmetry axes and rather has irregular shape and a large size. This type of diamond has usually formed under very high pressure for a long period of time [32, 37, 38].

Table 2: Levels of impurities in different diamond categories and manifestations forms of diamonds.

<b>Types of Diamond</b>	<b>Population</b>	<b>Impurity</b>	<b>Manifestation</b>
Ia	98.00%	Cluster form of nitrogen atoms	
Ib	0.1%	Scattered form of nitrogen atom	
IIa	1 – 2 %	Pure form of carbon	
IIb	0.1%	Some boron atoms	

**a) Type IIa**

Type IIa is also rare natural diamonds containing a negligible amount of impurities. Containing a few particles per million (PPM) of nitrogen that are not easily detected by infrared and ultraviolet absorption methods. Type IIa diamonds have erupted from the core of the Earth towards the surface of the earth. The intense pressure and temperature situation can cause structural rarity during the growth of the tetrahedral structure of the material. This imperfection in the crystal structure will produce colors such as yellow, brown, pink, orange and purple [33, 38].

**b) Type IIb**

All types of IIb diamonds are 1% – 2% of the natural form of diamond. Boron atoms are the main constituent of impurity in this type of diamond. The boron atom can absorb red, orange and yellow light and with shift the wavelength during emission so as to make the material appear as grey, blue or nearly colorless. Type IIb diamond has a p-type electrical activity due to the boron content in the crystal structure and 1 ppm is enough to show a semiconductor activity at room temperature with a hole mobility of  $1500 \text{ cm}^2/\text{Vsec}$ . The activation energy at room temperature is  $0.37\text{eV}$  [37, 38]. Table 2 above shows the different types of diamonds along with their populations and kind of impurities atoms involved.

**3.3 Description of Diamond Synthesization**

Synthetic diamonds are manufactured in the laboratory with specific grown conditions. The optical and chemical properties of synthetic diamonds are very similar to the naturally occurring diamonds [34]. The hardness of synthetic diamonds can vary, depending on the concentration of the impurities in the lattice structure, the difference of the atomic scale structure of the host material and the agglomeration the formation of the impurities due to the different growth environment. There are several methods for producing synthetic diamond, but typically, two methods are more commonly used to produce synthetic diamond due to their relatively low cost with a good quality.



### **3.3.1 High-Pressure and High-Temperature**

The importance of the high-pressure and the high-temperature (HPHT) methods has been significant for the growing process of synthetic diamonds. In 1955, H.T. Hall and his co-workers at General Electronic (GE) were the pioneers of this method [34, 39]. The basic idea was to compress graphite (another allotrope of carbon and an important precursor for synthetic diamond) with a hydraulic press along with liquefied metals until the carbon was transformed into the diamond crystalline form [30]. Metals like nickel (Ni), iron (Fe) and cobalt (Co) are commonly used for the graphite transformation process at an increased pressure range of 5 – 10 GPa and at a temperatures range of 1300 °C – 2300 °C [37].

During the transition process of turning graphite into the diamond form, the pressure has to be maintained at a certain level during transformation. The level of pressure in the developing chamber is very important for achieving good and pure synthetic diamond; otherwise, deviation of the pressure from a particular level would lead to a resultant form of diamond lattice that would convert itself instantaneously back into a graphite form. The final prepared form of synthetic diamond crystals obtained from the HTHP process is simply done by dissolving the metal in an acid [34, 41].

### **3.3.2 Chemical Vapour Deposition Method**

The chemical vapour deposition (CVD) technique refers to developing the solid materials while using the gas phase of a precursor at a suitable pressure and temperature. It is a useful and important technique for producing synthetic diamonds since the 1980s. This technique involves the gas phase of hydrocarbon radicals together with hydrogen atoms for deposition of carbon atoms on a substrate while using a hot filament under the CVD environment at conditions [42]. The conditions for the substrate requirements for this process will yield either the bulk form of diamond for homo-epitaxial growth or single crystalline diamond.

If the substrate is a non-diamond material, then an extra nuclearization step is required for growing hetero-epitaxial or polycrystalline diamond this way. The reason is that nuclearization provides a platform for the diamond seeds to grow in three-dimensional grains for further growing in a bulk form of synthetic diamond on non – diamond material. The CVD reactor is

typically filled with a gas mixture consisting of methane  $\text{CH}_4$ , and hydrogen with a ratio of (1:99) [37, 38]. The presence of the hydrogen gas in the chamber is necessary as the hydrogen will selectively etch the non – diamond carbon from the deposition area. The deposition rate, and the properties of the synthetic diamond, will depend upon the grain size and the  $\text{sp}^3/\text{non sp}^3$  ratio [42].

The synthetic diamond is used in a large number of applications such as microelectronics, optoelectronics, quantum photonics and quantum information processing. There are many other special applications for synthetic diamond in large scales such as for laser diodes, power semiconductor heat spreaders, high temperature diodes, thermistors, laser cooling crystals, solid-state detectors, grinding tools and for high power and high frequency electronics applications [43, 44, 45, 46].

**a. *Single Crystal Synthetic Diamond.***

A single crystalline diamond can generally be produced with homo-epitaxial growth. In this process, a large number of atoms are arranged in a periodical repetition of the atoms in a specific geometric structure of the volume for a solid material during the CVD. A diamond film fabricated by the homo-epitaxial technique is the purest form of diamond as compared to naturally occurring diamond.

The concentration of impurities, such as intrinsic and extrinsic defects, are in this case low and the measured value of impurities such as nitrogen  $1 \times 10^{15} \text{ cm}^{-3}$  and the dislocation density of atoms  $1 \times 10^6 \text{ cm}^{-2}$  are less than that of the natural diamond. The carrier mobilities are about 4800 and  $3800 \text{ cm}^2/\text{Vm}$  as measured for both electrons and holes respectively [36, 37]. A small size of CVD diamond of millimeter scale is produced using the homo-epitaxial growth.

**b. *Polycrystalline Synthetic Diamonds.***

A polycrystalline diamond film can be produced by using the technique called hetero-epitaxial growth process. The film is composed of single crystalline structures with a large number of inter-crystalline boundaries and defects. The concentrations of nitrogen and atomic dislocations are higher than that of the single-crystalline structure. The properties of these diamond films

depend upon the method for producing the diamond, the concentration of impurities, the inter-crystal boundaries and the geometric pattern of the structure and the environmental conditions inside the deposition chamber.

### ***3.3.3 Application of Polycrystalline and Single Crystalline Diamonds***

The applications of polycrystalline and single-crystalline diamonds are quite different in academic research as compared with in the industry. Poly crystalline diamonds are used in very high-power laser systems for high-speed cutting, writing and welding in many industrial manufacturing processes. The industrial tools made for controlling these high-power laser systems include beam couplers, beam splitters, specially designed lenses and objectives. CVD diamond has also some interesting applications in military defense systems. These diamonds are suitable for thermal imaging applications in very harsh environments. Other alternative materials for these thermal imaging applications in rough conditions require special protection treatment before installation.

Poly-crystalline CVD diamond is also a promising material for heat-seeking missile applications [38]. These diamonds are used when designing and creating spherical domes which have the ability to with stand erosion processes due to high-velocity impact of water droplets, dust particles, and insects at very high speed. Such diamond domes also have the ability to stand against aero-thermal heating effects upon launching the missiles [35, 37].

On the other side, single-crystalline diamonds are used for preparing optical products which consists of large variety of lenses, beam splitters, prisms and specially shaped lenses. This is because single-crystal diamonds have capability to be easily molded into a large range of geometric shapes as found in optical components.

### ***3.3.4 Damage and Defects of Diamond***

Damages and defects in the materials are generally due to the imperfections in the crystallographic structure of the materials. These imperfections in the crystals occur inside the lattice structure. The reasons for the damages and the defects in the lattices are details of both the extrinsic and

the intrinsic processes when growing the diamond in the laboratory or in the natural environment.

Damages and defects are created in the lattice structure in the form of for instance, missing an atom from the required position, dislocation of an atom in the lattice, dangling of an atom in the lattice and settling down of an alien atom in the lattice as a result of an intrinsic and or an extrinsic substitution process. These crystallographic defects will affect the properties of material the as the thermal, electrical, and optical the properties.

There are many different ways to detect these damages and defects in the materials. The most common techniques are electron paramagnetic resonance (EPR), examining the PL from these defects and damages, the absorption spectrum for visible, infrared (IR) and for ultraviolet (UV) light. The absorption spectrum of UV light is very helpful regarding finding the right estimation of the concentration for these damages and defects inside the material. Table 3 below, shows in detail the defects found in the different diamond categories.

Table 3: Different defect centers in different types of diamond [37, 38].

<b>Diamond</b>	<b>Defect Center</b>	<b>ZPL (nm)</b>	<b><math>\lambda_{em}</math></b>	<b><math>\tau</math> (ns)</b>
Type IIa	$V^0$	741	898	2.55
Type Ib	$N - V^-$	637	685	11
Type Ib	$N - V^0$	575	600	-
Type IaA	$N - V - N (H_3)$	503	531	16
Type IaB	$N - V - N (CH_2)$	415	445	41

## 4 NV COLOUR CENTERS IN DIAMOND

---

NV centers are optically active point defects in the diamond lattice and have recently become a very active topic for research in field of quantum photonics, quantum computing, highly sensitive magnetometry and quantum information processing [47, 48]. They are created by a pair nitrogen atom replacing a carbon atom and its nearest neighbor with a nitrogen atom at vacant point in lattice. The NV center consists of two charge states; a negatively charge state  $NV^-$  where an electron acts as a donor and neutral charge state  $NV^0$  where an electron acts as acceptors [48]. NV color centers are efficient source for single photon emitter at room temperature and are therefore very interesting and widely studied in nano photonic field.

### ***4.1 NV Centers in Diamond***

NV color centers can easily found in both Ia and Ib types of synthetic diamonds in the form of clusters and scattered atoms, but the concentrations and locations of individual color centers will be quite different from one piece of diamond to another. These defects can also be artificially formed by introducing the nitrogen ions into diamond through different ways such as, ions implantation and by introducing the nitrogen gas into the deposition chamber during CVD growth.

During the diamond growth processes, the growth rate depends upon the concentration of nitrogen  $N_2$  and methane gas  $CH_4$  in the deposition chamber and the symmetry of the lattice. The temperature of the substrate and pressure inside the chamber plays a crucial role during the deposition process, with the best quality CVD diamond being produced by homo-epitaxial growth under high pressure, high temperature HPHT condition, typically 1100 – 1200 °C and pressure of chamber is 150 – 200 Torr. The growth rate of diamond film can be increased by commencement of  $N_2$  &  $CH_4$  in gas phase into the chamber.

The color of diamond crystal are typically due to the presence of nitrogen atoms in the diamond lattice in the form of clusters and individual scattered atoms (See table 4 on page 21) [49, 50]. The addition of nitrogen ions during the deposition process results in an enhancement of growth

rate in [100] direction compare to the [110] and [111] phases. The incorporation of nitrogen in diamond acts as donor, it also affects the morphology and quality of crystal structure [50, 51].

Ion implantation is another simple way to introduce the nitrogen centers. This method directly implants atom into a material using an ion beam and is therefore independent of the atoms dislocation, solubility and diffusivity in the material. It is very attractive method for selectively introducing the impurities into crystals including the synthetic diamond. An ions implantation reactor is used to implantation where an ion beam is generated and directed towards the crystal. The concentration of impurities incorporated into the crystal depends upon the diameter of the ion beam, its flux and the total exposure time used will depend upon the required ion implantation dose in each material.

After ion implantation, annealing (typically at 800 – 900 °C) can be used to cause the implanted ions to diffuse further into the diamond and change their distribution. Annealing will also help to re-crystallize the diamond lattice, repairing the damage caused by the ion implantation process.

The position of the nitrogen atoms in the diamond lattice has a strong influence on their effect and the optical properties of the diamond material. Nitrogen atoms will replace individual carbon atoms in the diamonds tetrahedral structure with bond lengths of 0.77Å. By boron or phosphor doping diamond, the carbon atoms will be shifted from their equilibrium position which will also change the position of any nitrogen atoms present, and this can be used to engineer the materials properties.

#### ***4.2 Atomic Arrangement in Crystal Structure***

Solid materials that consists of an ordered atomic arrangement are called crystalline materials, most metals are including in this structure group. If this repeated form of pattern does not span over the entire macroscopic structure of the material, it is formed a polycrystalline structure. These structures can also be classified as simple cubic, body center cubic (BCC) and face center cubic (FCC) lattice structure. The simple cubic structure consists of four atom arranged at the each corner of the cubic structure.

The simple cubic structure consists of eight atoms arranged at the corners of a cube. This is known as its unit cell. The whole lattice structure is then built up from the repetition of this unit cell in three dimensions. Each atom is therefore shared with eight unit cells and the distance between two nearest neighbor atom is called the lattice length or lattice constant of the structure, denoted by ' $a$ ' in figure (4.1) which shows the unit cells of the simple cubic, BCC and FCC atomic structures.

In the BCC structure one atom is added at the center of the simple cubic structure, as shown in figure 4.1(b). If an extra atom is added to the center of each face of the simple cubic structure then the resulting structure is known as FCC structure as shown in figure 4.1(c) [49].

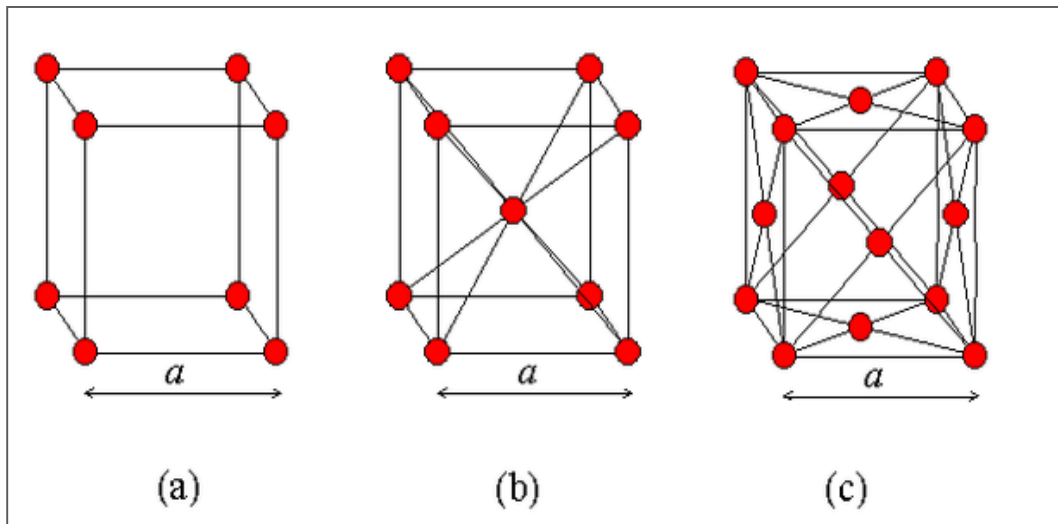


Figure 4.1: Structure of a unit cell for (a) simple cubic lattice structure, (b) body centred cubic, lattice structure and (c) face centred cubic lattice structure [49, 50].

The lattice structure of diamond is a combination of two FCC structures, one offset from the other by a quarter of a lattice constant, which is  $3.57 \text{ \AA}$  and hence the distance between two nearest neighbor is  $1.55 \text{ \AA}$ . The diamond structure is built up from the layer by layer combination of graphite structure with an offset between each consecutive layer, and is shown in figure (4.2).

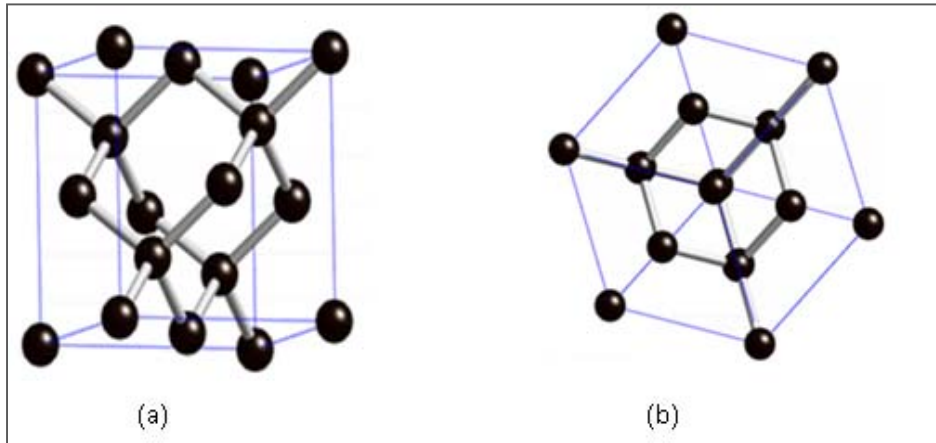


Figure 4.2: (a) Structure of the diamond unit cell with chemical bonds drawn between two nearest neighbour's atoms. (b) Diamond lattice structure after rotation of 30 in the x axis and 60 in the y axis direction [51].

### 4.3 Phonons

All the atoms in a solid material are locked in a specific position but can still move around this equilibrium position (vibrate). Energy can be associated with these vibrations known as the internal heat energy of the material. This energy can be quantized and the individual quanta are known as phonons.

Phonons are quasi-particle that propagates through a material at its internal speed of sound. The concept of phonons in solid materials was first introduced by Igor Tamm [53]. The amount of energy associated with a phonon can be described by the following equation.

$$E_{phonon} = \frac{h\nu_s n}{2L}$$

During the relaxation process of excited electrons in a material, energy can be released in form of both photons and phonons. In a two level de-excitation process that produces phonons, a broad photon emission spectrum will also be observed. Whilst a process that does not will produce a sharp Lorentzian shaped spectrum and is known as the zero – phonon line (ZPL) (see figure 4.4 on page 35).

The broad emission spectrum consists of two parts, first part represents the phonon sideband which actually comprises of many sharp discrete spikes and area under the curve is correspond to the phonon normal mode distribution. The second part of the spectrum showing the Lorentzian



distribution representing the energy released in form of photons during the de-excitation processes.

#### 4.4 Charge State of NV Centers in Diamond

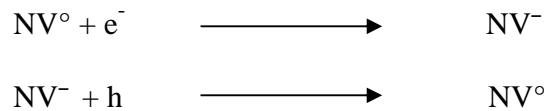
The nitrogen vacancy centers in diamond are useful defect for several reasons. They have applications in quantum computation, single spin magnetometry due to their ability for corresponding spin of the state. Diamond defects can also act as single photon emitters that are photo stable at room temperature shifting the wavelength in the visible range.

The optical properties of a diamond are completely depending upon the charged defects present in lattice and their concentration. The charge state of NV defects in diamond is highly dependent upon surrounding atoms in lattice. The presences of electron acceptors or donors in form of nitrogen ions with carbon atom in lattice will cause the implanted NV centers appear either in form of (NV<sup>°</sup>) neutral state or (NV<sup>-</sup>) negatively charged state respectively [52, 53].

Table 4: ZPL wavelengths and associated zero phonon energy of two charge-states of nitrogen vacancy centres in diamond.

Charge state	Zero Phonon line (ZPL)	ZPL energy (eV)
NV <sup>°</sup>	575 nm	2.15
NV <sup>-</sup>	637 nm	1.94

The following two equations show the creation and destruction of (NV<sup>°</sup>) neutral state or (NV<sup>-</sup>) negatively charged state respectively.



In order to get fluoresces from NV centers, samples are excited using the 532nm emission from a frequency doubled continuous wave Nd: YAG laser. The excitation laser power is adjusted to value less than 1mW to excite the NV centers in samples and focused to a spot size of ~ 10 μm diameter. Samples will contain both neutral and negatively charged NV centers depend upon the density of the centers in the nano-diamond powder used to prepare the sample.

Both states exhibit different ZPL wavelengths/energies under 532nm excitation (See table 4 and figure 4.4), and hence the emission peak in photo-luminescence (PL) spectrum from each center can be used to determine its charge state.

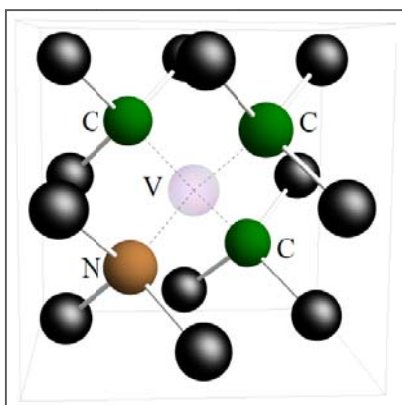


Figure 4.3: Structure of the nitrogen – vacancy centre in diamond, where nitrogen atom is shown in brown, nearest carbon atom to the vacancy shown in green colour and the vacancy is shown in white colour with a bonding with carbon atom [38, 52].

But it is very interesting as the power of excited laser is increased; the pursuance of photon bunching effect is more prominent in  $NV^-$  negative charge state as compare to the  $NV^0$  neutral charge state.

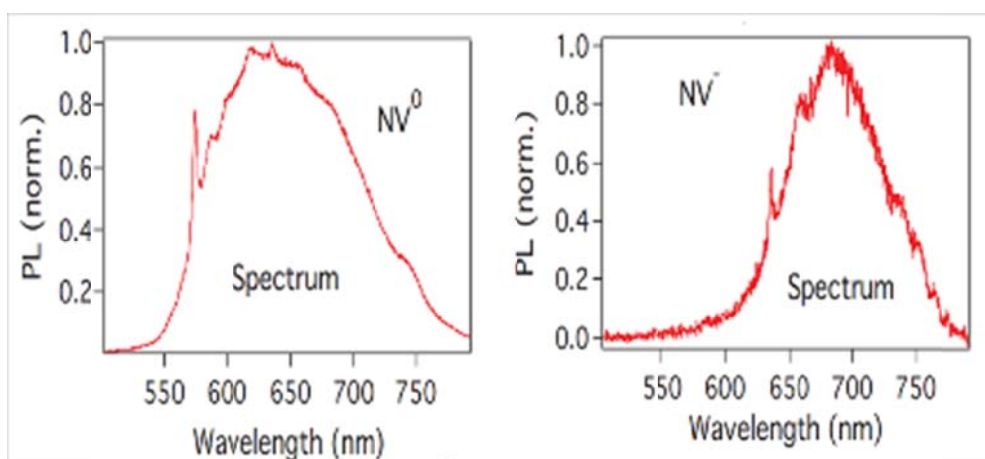


Figure 4.4: Traces of the spectrometer for each individual NV charge state [33, 52].

When NV centers are excited by  $< 0.5\text{mW}$  of pump light no photon bunching effect are seen for either NV charge states. But as the excitation power is increased, the photon bunching effect seen from the  $\text{NV}^-$  state becomes more pronounced compare to the  $\text{NV}^0$  state due to the  $\text{NV}^-$  state consisting of three energy levels including one which is meta-stable, which as the pump power is increased will start to become filled [52].

In case of  $\text{NV}^0$  neutral charge state, there exists no meta-stable energy level between the excited and ground state. All the electrons relax to ground state without temporally staying in the meta-stable level. The intensity of photoluminescence is much higher in  $\text{NV}^0$  neutral charge state, the property of fluoresces from NV centers are strongly dependent on the dipole orientation.

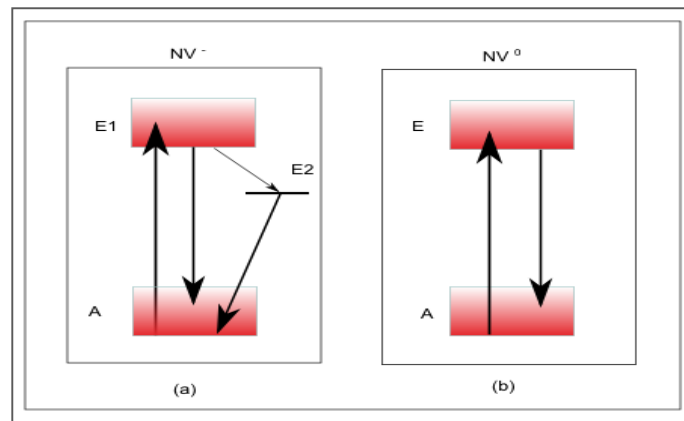


Figure 4.5: The energy level diagrams of NV centers. (a) The 3 – level structure of  $\text{NV}^-$  center showing a bunching effect at high excitation power. (b) The 2 – level structure of  $\text{NV}^0$  color center which is suitable for obtaining perfect anti-bunching curve at both high and low excitation power [33, 34, and 54].

#### 4.5 Energy Level of NV Centers

Both of the NV charge states produces an extra pair of electrons that interact with the carbon atoms in the diamond lattice to form an  $s = 1$  spin pair. This spin pair consists of two states which are denoted the ground ( $^3\text{G}$ ) and first excited state ( $^3\text{A}$ ) which lie within diamonds bandgap. Both the ground and excited states are triplet states, where are further split into three different sub-states having spin quantum numbers  $m_s = (-1, 0, +1)$ . The degeneracy between state  $m_s = 0$  and  $m_s = (-1, +1)$  is strongly depend upon orientation of the spin and the interaction

between the  $m_s$  sub-states. If the electrons have a high energy, it means that their spin are in the parallel direction ( $m_s = -1, +1$ ), and consequently if the electron have low energy it means that their spin will be anti – parallel ( $m_s = 0$ ). The degeneracy of the state ( $m_s = -1, +1$ ) is lifted when an external magnetic field is applied and the Zeeman splitting effect will then be seen.

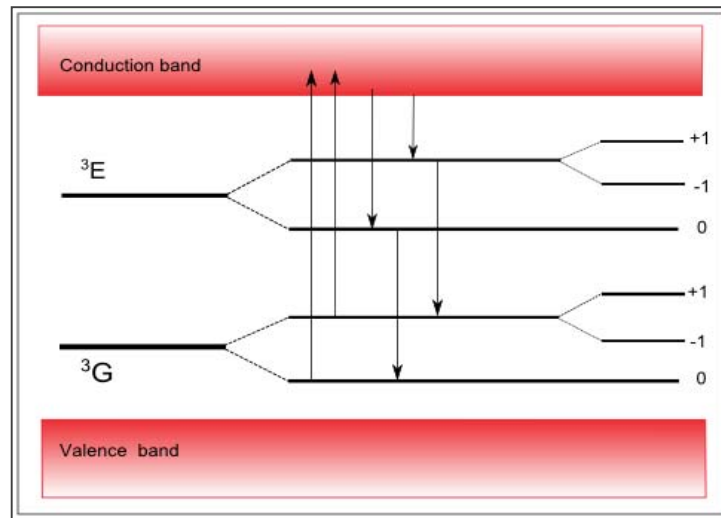


Figure 4.6: The diagram showing the energy level of nitrogen colour center consists of  $^3G$  grounds and the excited  $^3A$  state [34, 54].

As the sample is excited by 532nm photons, ground state electrons are excite into the conduction band. During their relaxation processes these electrons can non-radioactively relax into first excited state through phonon emission and then further relax to the ground state radioactively through photon emission. The spin state of the electrons is therefore preserved during the de-excitation process. The separation between the ground and excited states is 1.95eV, corresponding to a wavelength 637nm, however a large amount of emitted light is actually due to the phonon sideband, broadening the ZPL emission to 600nm – 800nm.

#### **4.6 Photo-chromic Effect of NV Centers.**

Diamond NV color centers are amongst the promising candidates for quantum information processing and qubits memories due to their unique properties. But, there are some optical properties of these color center that are not yet fully understood, such as photo-chromatic effects - a process where negative charge state are converted to neutral charge state. This photo-chromic

effect causes the bandgap to change and is a photon induced transformation that has been investigated in various studies [54]. According to Dumeige et al., the excitation of nano-diamond with femto-second laser would actually lead to transformation of NV color center first into  $NV^-$  color center along with  $NV^\circ$  color center and in last step of transformation processes the NV color center could appear as single stable  $NV^\circ$  color center.

Manson et al. explained this phenomenon as an ensemble of NV color centers, which verify that  $NV^-$  and  $NV^\circ$  charge state are a function of the excitation laser wavelength and the excitation time [52]. This photo-chromic effect is observed in all NV center containing diamond samples as they will all contain both  $NV^\circ$  and  $NV^-$  charge states. The behavior of the photo-chromic effect differs from sample to sample due to each sample containing different NV color center densities.

This photo-chromic effect is observed in all NV center containing diamond samples as they will all contain both  $NV^\circ$  and  $NV^-$  charge states. The behavior of the photo-chromic effect differs from sample to sample due to each sample containing different NV color center densities. This diverse behavior of photo-chromic effect is needed to investigate the photoluminescence from  $NV^\circ$  and  $NV^-$  color centers separately by using the spectrometer traces for each of individual charge state. The photo-chromic effect can be observed in the bulk form of diamond if the sample is first excited with low excited power then later the power of excitation laser increases. The photoluminescence of  $NV^\circ$  color center is stable at low power but the dominances of PL from  $NV^-$  increases as excitation power increases. This is a sign of transition from  $NV^\circ$  color center to the  $NV^-$  color centers by increasing the excitation power [52].

## 5 SAMPLE PREPARATIONS

---

Many different techniques for the preparation of optical trapping sample have evolved over the years, but the sample preparation technique used here is a relatively simple one. Diamond powder purchased from Element Six is dispersed in de-ionized (DI) water and this is then investigated. The powder used was synthetic type Ib diamond with 0.1% nitrogen concentration.

The average size of the nano-diamond particles in the powder was  $250 \pm 5$  nm and the number of NV centers in each nano-diamond was ~500 ppm. About 0.5ct = 0.1g of nano-diamond powder was mixed into 50ml of DI water and then centrifuged at 2000 rpm for 2-3 minutes, to completely mix the nano-diamonds into the water. The amount of 10ml colloidal aqueous solution containing suspended particle of diamond is asunder from rest of colloidal aqueous solution for the purpose of sample preparation.

A drop (~0.1ml) of colloidal solution was then deposited on the center of a 25 x 25mm glass cover slip. The sample was then left overnight so that the DI water could evaporate and allow the nano-diamonds become deposited on the surface of glass cover slip. This process can be accelerated by heating the sample on a hotplate for 2-3minute for evaporation but this will affect the distribution of the nano-diamond particles. Once all the DI water has evaporated, the sample is ready for use.

To prepare samples for optical trapping experiments, a nano-diamonds particle suspension was bought from Adamas Nanotechnologies Inc. The suspension contains 0.1 - 10% synthetic nano-diamond particles suspended in DI water. Sample were prepared by carefully placing a drop (0.1ml) of the suspension at the center of a 25 x 25mm<sup>2</sup> glass cover slip, and then placing another cover slip directly on top of this, to encapsulate the drop. The two cover slips were then fixed together using adhesive clear plastic tape. This technique was used as it reduces the rate at which the DI water evaporates and therefore increases the amount of time each sample can be investigated for. A schematic of the sample preparation technique used for optical trapping

samples is shown in figure 5.1 (a). Figure 5.1 (b) shows an optical image of a sample after it has been prepared.

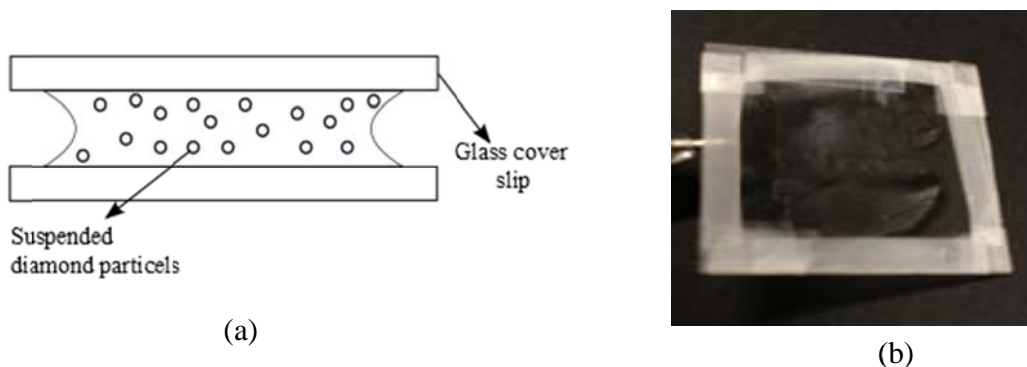


Figure 5.1: Representing the technique for the sample preparation and the prepared sample itself. The image 5.1(a) consists of the schematic diagram of the optical tweezer sample and image 5.2 (b) shows the real sample.

The zeta potential of the prepared solution was  $-35\text{mV}$  and pH level for a 10% mass of aqueous solution is 4 – 5. For optical trapping, the viscosity was 15 -20 cP and density of particles was about  $0.96 - 2 \text{ g/cm}^3$  at  $20 \text{ }^\circ\text{C}$ . These values of viscosity and density play a key role in determining and balancing the optical forces on the particle and were therefore carefully controlled.

## 6 EXPERIMENTAL SETUP

---

For this work a custom designed and built dual-beam confocal microscope system was constructed. The most crucial part of the experimental setup was the design of the dual confocal microscope 'sample holding platform', which needs to be capable of optically addressing a single nano-diamond particle without any drift and therefore needs to have a very high resolution, (see table 5).

The microscope setup also needs to be able to efficiently collect the photo-luminescent (PL) light emitted by a excited material and then transmit it using an optical fiber to the other parts of the experimental set-up so that it can be measured using either a spectrometer. This custom designed microscope system also has the capability to trap the nano-diamond particles.

### **6.1 Confocal Microscope**

An optical microscopy is a device used to study the microscopic structure on an object. There are certain limitations associated with an optical microscopy, such as its resolution and depth of focus, which make task such as true 3D imaging impossible for a convectional optical microscopy. However confocal microscope systems can avoid many of these limitations by using a small illumination spot and then by scanning a sample in x-y plane [59, 60]. The information gathered by this confocal setup is then process to build up an image of the entire sample.

The first confocal microscope was proposed by Marvin Minsky [58, 59]. The qualities of the images obtained are improved by excluding the light from outside the microscope's focal plane, which dramatically improves the images contrast when compared to a conventional microscope. The modern form of confocal microscope is highly modified from the original version proposed by Minsky, but the principles of confocal microscopy remain the same [59, 62]. Figure 6.1 shows a schematic diagram of the dual beam confocal microscope used here.



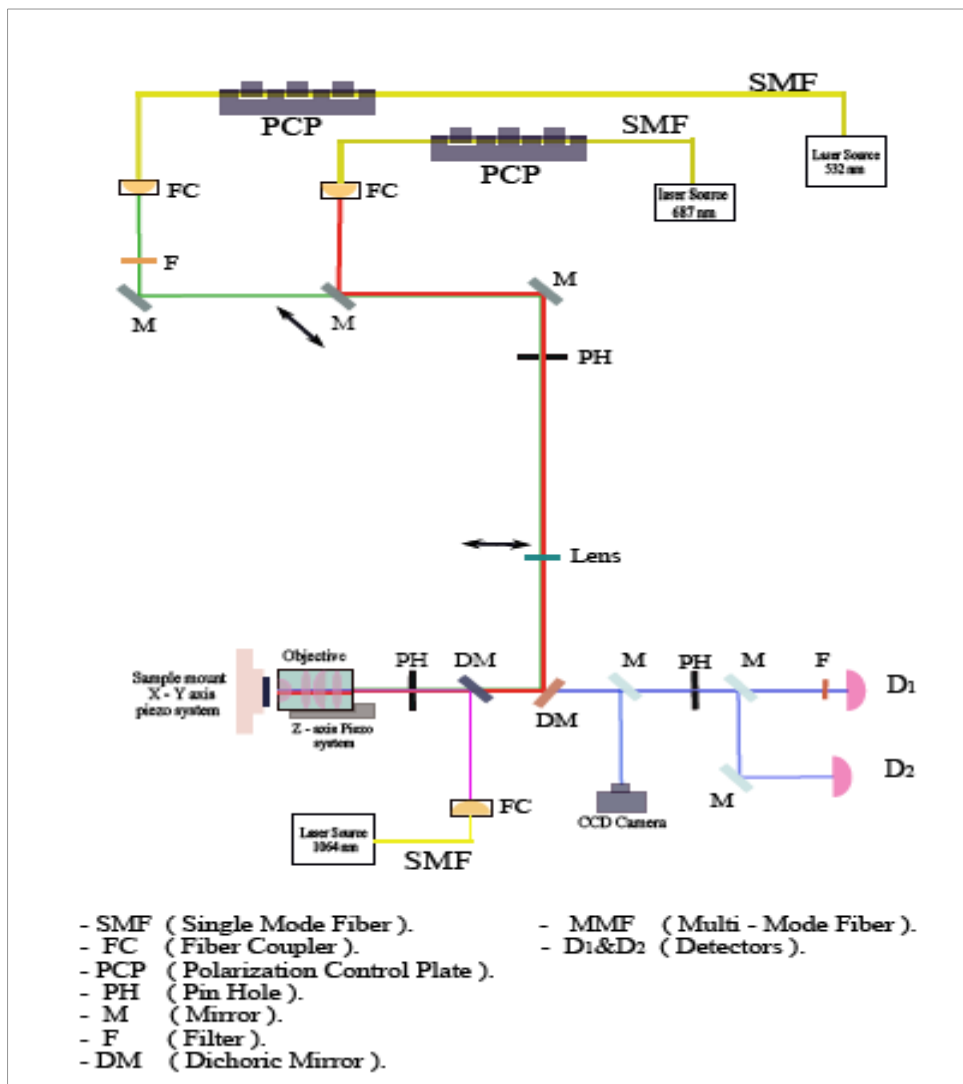


Figure 6.1: The schematic diagram of a dual confocal microscope used for imaging the defects in diamond, QDs of CdSe and TDBC molecules. This setup is also used for OT of diamond particle doped with nitrogen.

The minimum feature size a confocal microscope can image depends both upon the magnification power of the objective used and minimum step size of the piezo-system used to raster scan the sample. The resolution limit of dual confocal microscope can be determined for both of the excitation lasers used by the equations in table 5, where ' $\lambda_{exc}$ ' is the excitation wavelength, ' $n$ ' is the refractive index of the sample medium and NA is the numerical aperture of the objective.

Table 5: Calculated value of lateral, axial and confocal resolution of confocal microscope for the 532 nm and the 687 nm excitation laser system.

$\lambda_{exc}(nm)$	NA	Lateral Resolution $r = \frac{0.61 \times \lambda_{exc}}{NA} \text{ nm}$	Lateral Resolution (confocal) $r = \frac{0.4 \times \lambda_{exc}}{NA} \text{ nm}$	Axial resolution $r = \frac{1.4 \times n \times \lambda_{exc}}{NA} \text{ um}$
532	0.95	342	224	1.98
	1.3	249	164	1.05
	1.4	232	152	0.91
687	0.95	441	289	2.55
	1.3	322	211	1.36
	1.4	300	196	1.17

### 6.1.1 Laser source

A laser is used to excite the impurity, ion, atom or dye molecule of interest in the host material. The excited impurity or molecule will then emit light at a lower energy (red shifted) wavelength through a process termed PL (phosphorescence/fluorescence). Photo-luminescence (PL) is caused by excited photo-carriers in the sample material returning to their ground state through a radioactive process. Non-radioactive recombination is also possible but will not obviously be directly observable.

The excitation wavelength used will depend upon the absorption spectra of the material under investigation. In the dual beam system used here, two different excitation sources are used so different types of sample can be excited without needing to change the set-up. The excitation sources used are: i). A CW frequency doubled Nd: YAG laser emitting at 532nm, and ii). A semiconductor laser diode emitting at 687nm.

### 6.1.2 Mirrors

Mirrors are an important part of a microscope setup. In the dual-beam microscope system silver polished mirrors are used in the setup as they have a high reflectivity across a broad wavelength region (reflectivity > 96% between 400-700nm and 97.5% between 700-2000nm). The mirrors have a silver coating deposited on one-side with a flatness of  $\lambda/4$ . The thickness and the diameter

of the mirrors was selected to be 25mm and 6mm respectively to both provide flexibility for beam steering and for practicality reasons.

### **6.1.3 Pinhole**

The role of pinhole in confocal microscope setup is to improve the image resolution, quality and depth of focus. There are two important reasons to use a pinhole in a confocal setup, firstly the pinhole will 'reject' any light that is not being collected from the objective focal plane (front focal plane) and secondly removing the higher order diffraction rings of the Airy disc. Both of these effects will improve the contrast (signal to noise ratio) of the corresponding image.

Pinholes were also used in the construction of the system to control the height of the beams passing through the system by measuring the intensity of light passing through the pinhole at various points around the system. As such pinholes are also an important tool for maintaining the different lasers beam at a same optical axis of the microscope system.

### **6.1.4 Objective**

A microscope objective is an important optical element in microscope system, consists of one or more lenses and mirrors that act as an ideal lens. The objective is designed such that all the lenses are mounted in the same cylindrical tube and chosen such that their individual aberration will cancel out each other. The main role of the objective in microscope setup is to focus the excitation beam onto the sample and then collect the re-emitted light in order to create an image of the sample. The resolution of the image obtained is dependent upon the value of numerical aperture (NA) and magnifying power of the objective used.

An objective can be considered as a single lens with a focal length,  $f$ , and numerical aperture, NA. The maximum light emission angle ' $\alpha$ ' that can be imaged from a point on the sample can then be determined using equation (6.1).

$$NA = n_g \sin(\alpha) \quad (6.1)$$

Where  $n_g$  is the refractive index of cover glass typically equal to 1.5. So, according to Snell's law we can write,

$$NA = \sin(\alpha') \quad (6.2)$$

The value of lenses numerical aperture is dependent upon its diameter and focal length. If the value of a diameter is greater than the focal length then the value of numerical aperture is equal to the unity which follows the relation ( $NA=d/2f$ ). Introducing the oil between the objective and cover glass slip will add factor of  $n_{oil}$  to the relation in equation (6.1) and hence increases the effective NA of the lens by removing the limitations on the objective regarding the magnification power. The numerical aperture can be written as,

$$NA = n_g \sin(\alpha) = n_o \sin(\alpha) \quad (6.3)$$

Where  $n_{oil}$  is the refractive index of oil. A good objective with high resolution is called immersion objective. It is designed in such way that refractive index of glass can match the refractive index of oil to attain the value of numerical aperture 1.4. The value of numerical aperture for oil immersion objective is derived as,

$$NA = n_o \sin(\alpha)$$

By inserting the value of ' $\alpha$ ' in equation,

$$NA = n_o \sin\left(\arctan \frac{D}{2f}\right) \quad (6.4)$$

$$\approx \frac{D}{2f} \quad (6.5)$$

Similar equation can be written for an objective without oil  $NA = \sin(\arctan D/2 \times f)$ , by assuming that the cover glass slip is very thin. So, the value of numerical aperture is  $NA \approx \frac{D}{2f}$ .

The NA is very important for microscope, because it determines the brightness of image, depth of focus and spatial resolutions. The brightness of the image formed is equal to  $NA^4/MAG^2$ , hence a higher NA lens with the same magnification will result in a brighter image and vice-versa. The objective also determines the depth of field imaged by the relation  $\lambda/NA^2$ .

### **6.1.5 Filters**

Filters are coated transparent or partially transparent pieces of glass that can transmit or blocks specific wavelengths of light. Filters can be placed in the path of the collected PL light to block the pump and any unwanted light which has been transmitted by the pinhole. Filters only allow the specific wavelength of fluorescence that pass through it. This will again increase the signal-to-noise ratio of the collected light and improve the results without any pump.

### **6.1.6 Detectors**

A single-photon avalanche photo-diode (SPCM–AQR–13, PerkinElmer Optoelectrics<sup>1</sup>) was used to count the number of PL photons emitted by the samples. These specially designed detectors have photon detection efficiencies of around 65% at 650nm by utilizing 180 $\mu$ m diameter silicon active elements. The intensity of the signal generated by the detector corresponds to the number of photons striking the detector and therefore allows the number of photons emitted in a selected time interval to be determined.

The detectors used in the system have the ability to count up to 5 million photons per second (Mc/s) with dead time of 35 – 50ns between pulses. The detector efficiency varies across the 400 - 1100nm range but peaks at around 650-700nm. A single pulse from a detector corresponds to 104 photons with dark count of 250 photons and the width of each pulse is 1ns.

### **6.1.7 Optical Fibers**

Optical fiber carries light along their core, which is surrounded by a cladding material with a slightly lower refractive index (typically  $\sim 1.51$  vs. 1.50). Light therefore travels from one end of fiber to the other through total internal reflection. In planar material the angle of total-internal reflection is relatively easy to calculate, but for optical fibers things are complicated by the cylindrical geometry.

However table 6 details the number of modes that will propagate along a series of fibers. The process of total internal reflection depends upon the angle of incidence  $\theta_i$  from one medium to

---

<sup>1</sup>For more details about the PerkinElmer photon detectors visit website [www.perkinelmer.com](http://www.perkinelmer.com) and check the data sheet of the (SPCM – AQR – 13) detector (accessed on July 15, 2013)

the angle of refraction  $\theta_r$  in another medium. The minimum value of angle of incidence requires to produce the total internal reflection is called critical angle  $\theta_c$ . So according to Snell's law,

$$n_1 \sin \theta_i = n_2 \sin \theta_r$$

So, for critical angle  $\theta_i = \theta_c$  and  $\theta_r = 90$ , then

$$\theta_c = \sin^{-1}\left(\frac{n_2}{n_1}\right) \quad (6.7)$$

Table 6: Number of modes propagating along the MMF and SMF fibre for different values of core diameter.

Type of Fiber	Core diameter d (um)	NA	Wave length ( $\lambda$ nm)	Number of modes $N = \frac{1}{2}((\pi d \times NA)/\lambda)^2$
Multi – Mode Fiber	25	0.1	750	54.8
	50	0.22	600	1061.1
	50	0.22	750	1658.01
Single – Mode Fiber	3.6	0.13	532	3.81
	4.6	0.12	680	3.25
	6.2	0.14	1064	3.28

The refractive index is most important parameter for fiber, because light can travel through material that is used in the core of fiber. In order to keep the light inside the core of fiber than cladding material with high refractive index ( $n = c/v$ ) is used. There are two most important and commonly used types of fibers, one which can propagate many paths along the core known as transverse mode is called multi – mode fiber while the other can only restricted to support the single way of propagation is called single mode fiber. Number of modes propagate through the fiber is calculate as,

$$N = \frac{1}{2}(\pi.d.\left(\frac{NA}{\lambda}\right))^2 \quad (6.8)$$

Where 'd' is diameter of fiber core, 'NA' is a numerical aperture and ' $\lambda$ ' is the wavelength of light propagating through the fiber. The diameter of multi – mode fiber is much greater than the diameter of single mode fiber. The table 6 is showing the number of modes propagate through

MMF and SMF with different core diameters. Fibers come in a variety of different forms, but are typically divided into two groups, single-mode and multi-mode.

**(a) Multimode Fiber**

Multimode fibers have large core diameters and can therefore support many optical modes, i.e. the light propagate along the fiber can follow many different paths. The large core diameter gives rise to the fibers having large numerical apertures and allows a large amount of light to be easily coupled into and out of these fibers.

However their multi-mode nature gives rise to a number of problems relating to pulse broadening due to the different in time light in the different modes will take to pass through the fiber and the beam profile emitted by the fiber. These limitations make their use in microscopy applications more problematic but they can be used when high-coupling efficiency is a necessity.

**(b) Single Mode Fiber**

Single mode fibers are designed to support only one optical mode in their core and are therefore relatively wavelength specific. The negligible modal dispersion experienced by light pulse propagating in the fibers (when compared to multi-mode fibers) make them ideal for long -range telecommunication applications.

$$v = 2\pi a \left( \frac{NA}{\lambda} \right) \quad (6.9)$$

In order for a fiber to be single mode, its normalized frequency ‘ $v$ ’ (as defined in equation 6.9, where ‘ $\lambda$ ’ is free space wavelength and NA is the numerical aperture of fiber core) must be less than 2.4. Otherwise the fiber will support multi-mode operation [57, 63]. If a value of normalized frequency exceeds from 2.40 which is suitable for multimode fiber. In MMF, the light can propagate in superposition of all modes confine into the cone which defining the NA of fiber. But in case of SMF single mode of light can propagate through the core of fiber

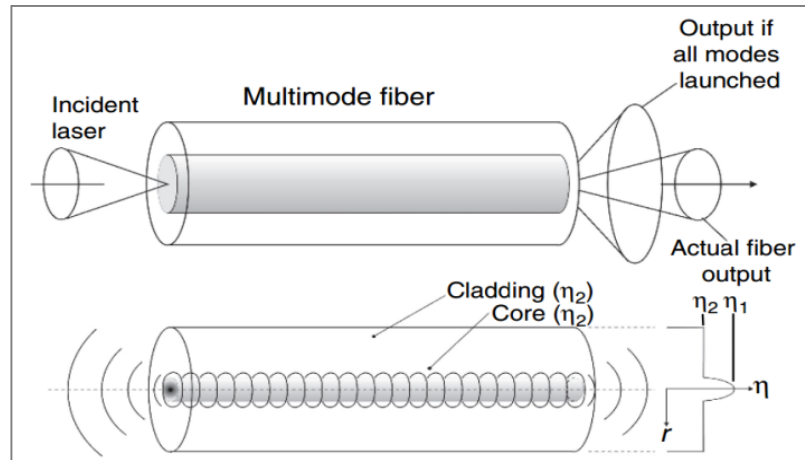


Figure 6.2: The diagrammatic representation of the difference between the MMF and SMF fiber for propagation of light from the core [58, 63].

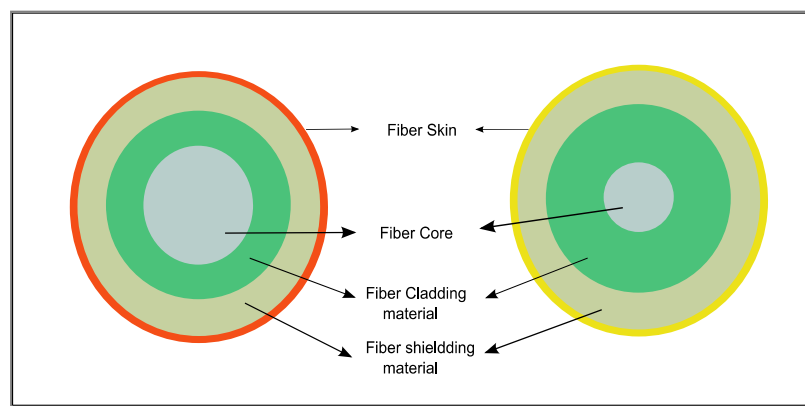


Figure 6.3: The picture showing the structural diagram of a multimode fiber (MMF) and a single-mode fiber (SMF). Orange and yellow color represent the protective plastic skins of MMF and SMF.

### 6.2 HBT setup

The Hanbury-Brown and Twiss setup is used to measure the photon number statistics and specifically to measure the signal generated by the collected photons during the particular excitation time interval.



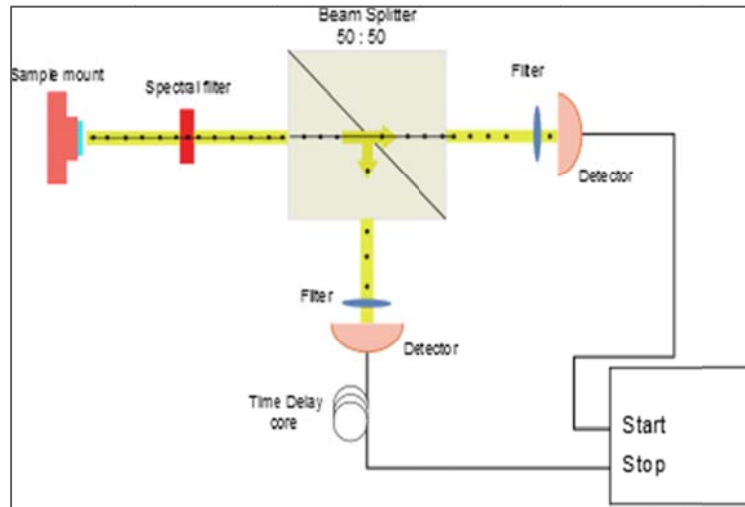


Figure 6.4: The schematic diagram of the HBT setup used to calculate the value of the second-order correlation function, showing the start and stop values for  $g^2(\tau)$  function for drawing the antibunching curve.

The basic idea behind this HBT experiment is that measuring the intensity fluctuations of a light beam, which is related to its coherence. If the incoming beam of light in HBT setup strikes two detectors it is coherent then the fluctuation in the beams will be correlated with each other. The modern HBT setup consists of a beam splitter which could be polarized and un-polarized depending upon the fluorescence polarization properties of the collected from sample by microscope setup. The beam splitter divides the collected signals into two paths and each signal are then lead to a photon detector. The selection of detectors is very important regarding the wavelength of fluorescence collected from the setup.

If the collected fluorescence is in visible range so silicon APDs are used with having some dark counts and have good efficiency. The figure 6.4 is showing the custom built HBT setup. By measuring the correlation between the intensity fluctuations, one can easily measure the coherence property of light with HBT setup rather than to perform the interference experiment.

### 6.3 Spectrometer

In the process of light matter interactions a spectrometer is an important instrument to analyze the fluorescence emitted from material. A spectrometer disperses the light incident on it using a diffraction grating and then measures the intensity of a small range of this dispersed light. By then scanning the measured range across the entire wavelength range of interest, it is possible to build up a complete spectrum for a light signal. A single 1800 lines/mm grating spectrometer

was used in the microscope system built for this project and was used to measure spectra for all the samples investigated. These spectral lines used to identify the material which is actually shifting the wavelength from incident light to reflected light. Spectrometer is useful for a small portion of electromagnetic spectrum rather than the whole spectrum range from gamma to the far infrared region.

During experiment, a custom built spectrometer was used to analyze fluorescence spectral lines. Spectral lines are different for different analyzed materials which consist of sharp peak at certain wavelength and these sharp peaks in the spectral lines are indicating the emission from material at that particular level of wavelength in EM spectrum.

#### **6.4 CCD Camera**

A charge coupled device is an important tool of digital imaging technology. A CCD camera consists of an array of p-doped metal oxide semiconductor (MOS) capacitors, which act as image sensors. The intensity of electrical charge produced in the capacitor is proportional to the intensity of the incident light striking it and therefore by measuring all the capacitors in the array it is possible to build up an image. The creation of image is an accumulation process of electrical charges from each capacitor into dimensional array (one dimensional array for line scanning and two dimensional arrays used for video and still image capturing). Later in this process, the electric charge finally converted into the voltages to feed the digital devices. The image can processed through variation in voltage due to the electric charge.

The quality of CCD camera images depends upon the size and type of the sensor and the quality of its optics. Incident light is focused on to the surface of the CCD sensor using a series of lenses and it is important that these lenses are of a high quality if a high resolution image is to be obtained. The area of CCD sensor also affects the brightness and magnification of the resultant image, such that if a CCD camera has small individual sensors it will produce a higher resolution image but will collect less light resulting in a lower brightness. But, larger the area of sensor means more light focused on it which provides the high brightness and poor resolution in image. The design and the type of CCD sensor are also very important for digital imaging.

### 7.1 Testing the Microscope Setup

After constructing of the dual confocal microscope setup was completed on smart table, it was then characterized using a simple microscopic structure. A diffraction grating with grating period  $1\ \mu\text{m}$  was placed on the sample holder for this purpose. Figure 7.1 shows CCD camera images of the diffraction grating in a normal mode. The image 7.1(a) shows the central the part of diffraction grating, whereas the image 7.1 (b) shows the starting point of the diffraction grating lines on the substrate strip. Both these images are circular because images are taken using wide field of illumination with 100x (NA = 0.75) objective.

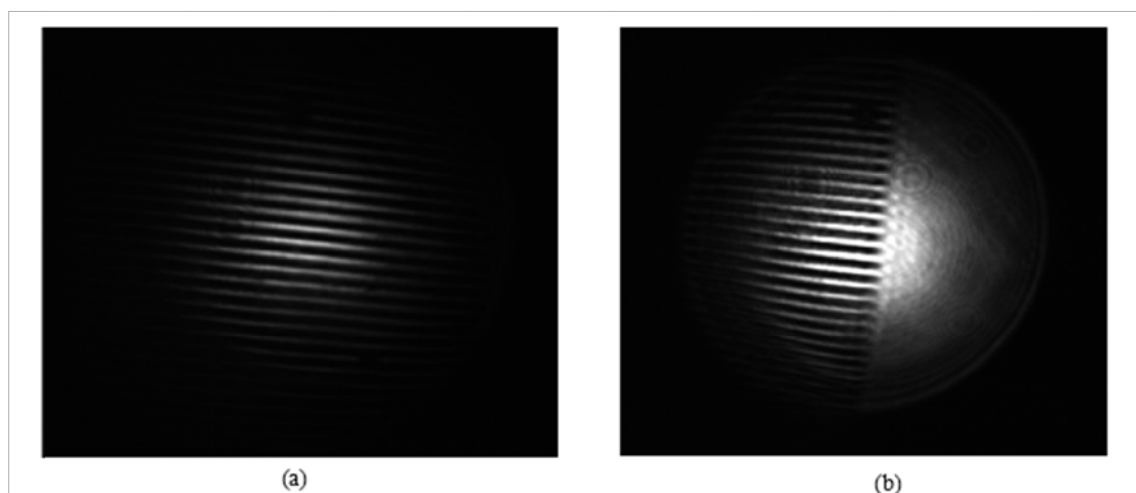


Figure 7.1: The image of a diffraction grating at a widened field illumination is taken with a CCD camera.

The most important part of the characterization process was determining the focal point of the system and this was achieved by scanning the grating (sample) in the z-axis. After the focus point had been determined using normal illumination mode, the microscope was then ready to be used in confocal mode. For confocal mode the objective used was changed to a 100x magnification (NA=0.90) objective to achieve higher resolution.

In confocal mode operation, raster scanning is performed by the microscope setup in the x – axis and y – axis directions to illuminate each point on the sample and then combining all of the data from each point to form an image. Figure 7.2(a) shows an image obtained in confocal mode with NA = 0.90 at a focus point of 48 $\mu$ m.

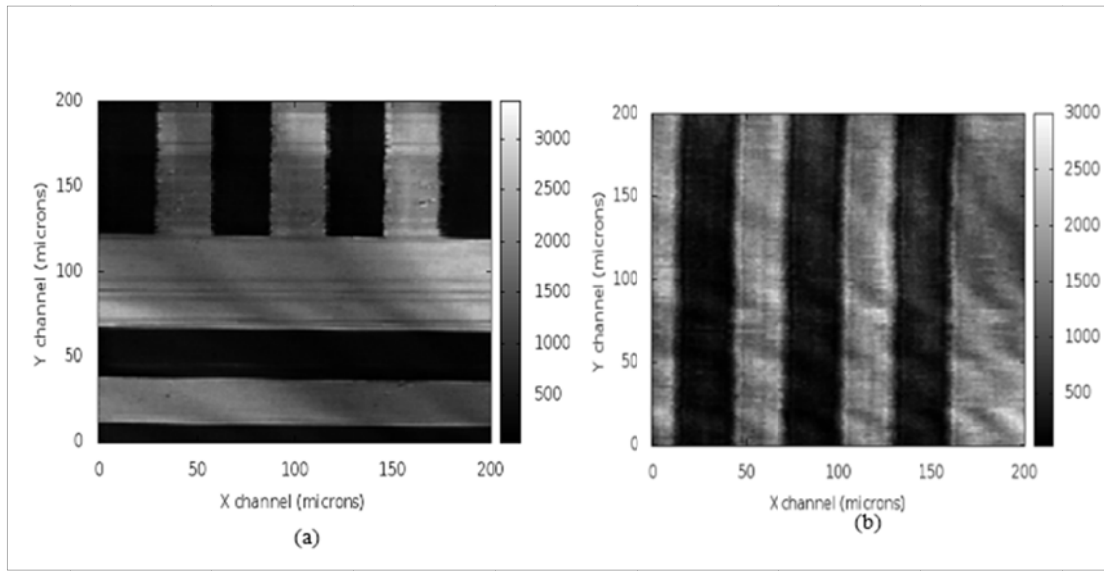


Figure 7.2: The figure showing the results of the confocal microscope scanning. The images (a) and (b) shows the different portions of the diffraction grating pattern scanned with different values of the focus points using 2  $\mu$ W of pump laser.

Figure 7.2(b) shows a different area of the grating, the focus length has been changed to 86.85 $\mu$ m to increase the number of counts measured and improve the contrast of the image. However it is clear that the image in figure 7.2(a) is brighter and more detailed than 7.2(b), as would be expected from moving the diffraction grating away from the focal point of the microscope system. This suggests that there is a slight difference in the focal point of the excitation and the image resolution. The figure 7.2 is an image of confocal mode scanning of microscope and it was observed from the scanned results that the microscope had been working well during the confocal mode scanning.

### **7.2 Scanning of NV Color Center**

The scanning of NV color centers in diamond was performed after replacing the diffraction grating with NV color centers sample in sample holder. This task was performed by using the oil

objective 100x/1.3 in order to get the maximum resolution of the microscope setup. Figure 7.3 shows images of some bright spot, where each bright spot in figure 7.3(a) represent a series of individual or groups of NV color centers.

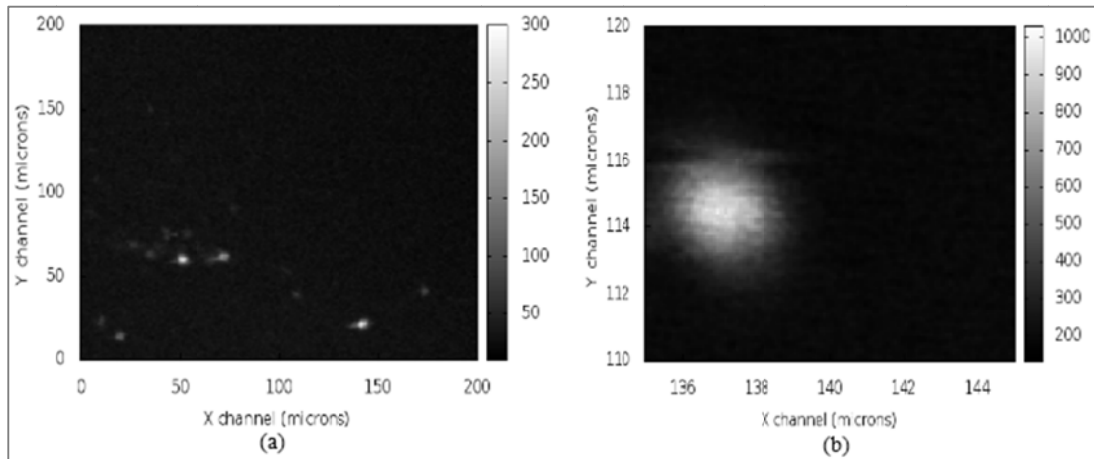


Figure 7.3: Results of broad-area scanning of the NV centers in diamond (a) Image of a few NV centers obtained during broad-area scanning of  $200 \times 200 \mu\text{m}^2$  (b) Image of single NV centers in diamond particles obtained during a fine area scanning of  $10 \times 10 \mu\text{m}^2$ .

The information about the size and shape of randomly selected any bright spot from broad area scanning image was precisely collected during the fine area scanning of that particular bright spot. Figure 7.3(b) is an image of a single NV color center which is producing the more than 1000 photons counts per 50ms integration period (20000 C/sec). As such this NV color center is a suitable candidate to measure using the HBT setup to check for anti-bunching behavior, as a minimum count rate of 15000 – 20000 C/sec is needed for this measurement to be possible with the set-up available.

### **7.3 Scanning for Different Samples**

The microscope was also used to look at some other samples. Figure 7.4 shows the images obtained from a series of colloidal Cadmium Selenide (CdSe) quantum dots. Bulk form of CdSe has a bandgap of  $\sim 1.7$  eV at 300K and therefore CdSe QDs will absorb 532nm very strongly. As the quantum dots are nano-structures the emission wavelength of the individual dots will be blue shifted relative to the bulk bandgap figure and hence these dots emit in the 650 – 655nm

wavelength range. The images were obtained using the NA=0.9 objective, 250 $\mu$ W excitation power and a focal length of 53.2 $\mu$ m.

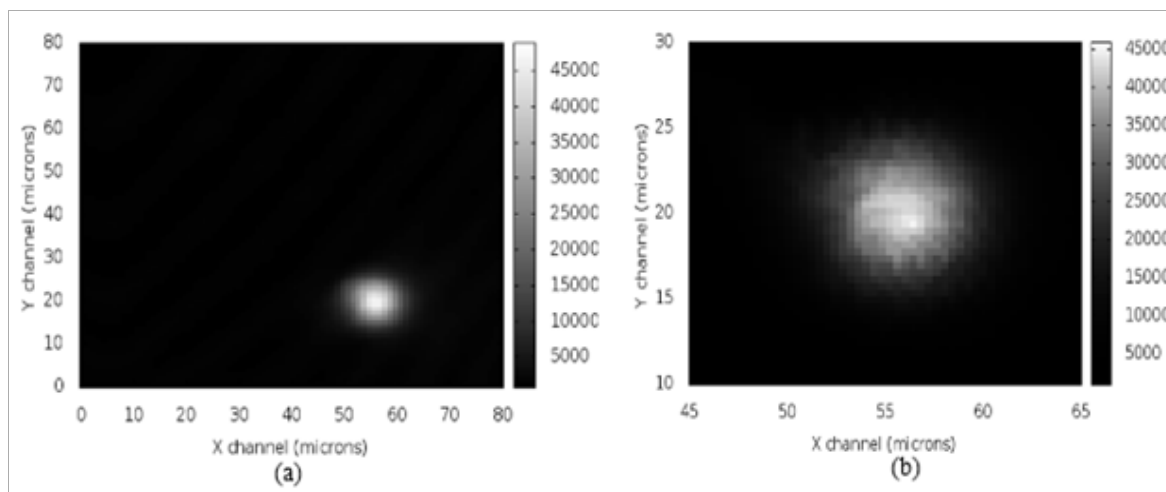


Figure 7.4: Scanning results of QD (CdSe) samples in broad-area scanning of 80 x 80  $\mu$ m<sup>2</sup> and a fine-area scanning of 30 x 30  $\mu$ m<sup>2</sup>.

Agglomeration (clumping) can occur for aqueous solution of CdSe QDs if the zeta potential is larger than the standard mean value. If the value of zeta potential is very small for solution than the size of QDs remain stable. The scanning of QDs was performed with the same 100x (NA=0.90) objective by using the 532 nm cw lasing system with 250  $\mu$ W excitation laser power. The absorption of CdSe QDs was around visible green wavelength and emission spectrum of QDs was also in visible red color regime. The wavelength shift of the CdSe QDs are size dependent of QDs. The absorption wavelength of the QDs was calculated by the following equation.

$$E = \frac{\hbar c}{\lambda}$$

The energy of absorbed photon is inversely proportional to the wavelength. The images in figure 7.4 appear to show that the QDs have diameters of is about 8 – 10  $\mu$ m, but this is actually due to the agglomeration of the QDs due to zeta potential of the solution. There are two reasons for agglomeration process of QDs. If the chemical reaction in aqueous solution is unstable than agglomeration occur in form of gathering the QDs at a single point. The other reason is the value

of zeta potential away from the stable value of solution containing the self-assembled QDs. The value of the zeta potential is solely dependent on the surface charge of nano particles.

Until now, the scanning of the specimen was performed with 532 nm laser. In order to test the performance of the microscope using the 687nm excitation source a TDBC polymeric molecule sample was imaged. Scans were performed at very low excitation powers, 10 $\mu$ W. The images in figure 7.5 show the results of these measurements and show a series of clusters of polymeric molecules. The images were obtained using the NA=1.3 oil immersion objective. The scanned image is showing the cluster form of polymeric molecules in white color. The visibility of custom built dual confocal cannot go beyond the diffraction limit (see table 6 on page 42) and we know the size of single polymeric molecules is less than 10 nm.

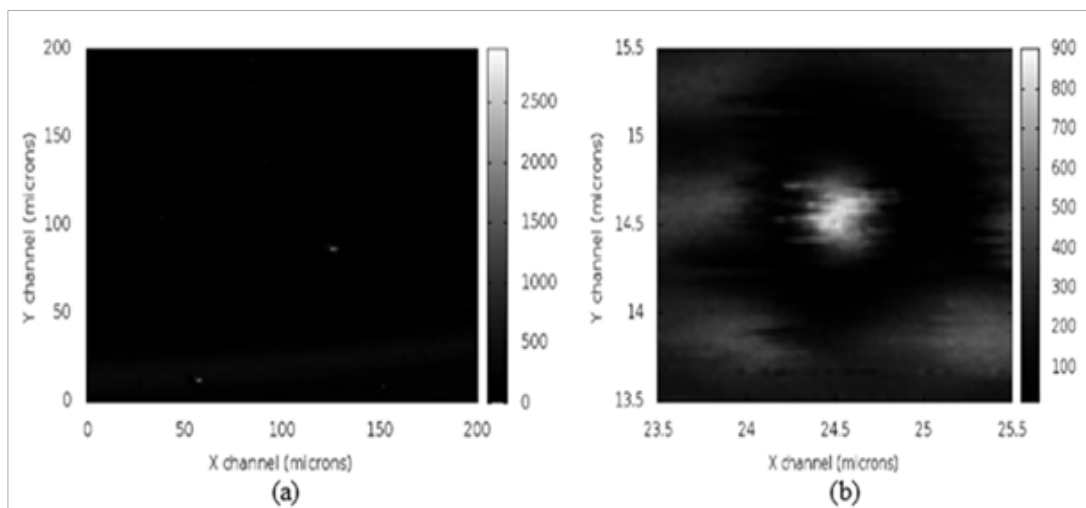


Figure 7.5: The scanning results of the dual microscope setup by using the 687 nm laser. (a) Image of a broad-scanning the sample in a 200 x 200  $\mu\text{m}^2$  area. (b) The image of fine scanning of the sample in a 2 x 2  $\mu\text{m}^2$  area with different value of the focus.

Figure 7.5(a) shows a broad area scan with some bright spot indicating molecules producing more than 2500 photon Counts per 50msec integration period. The formation of molecules cluster is confirmed during the fine scanning performed on 1 x 1 $\mu\text{m}^2$  area around a randomly selected bright spot as shown in figure 7.5(b).

#### 7.4 Results of Optical Trapping

A Nd: YAG 1064nm laser source was used to trap particles. This 1064nm source was selected for trapping the particles as the photons low energy reduces the chances of the photons being absorbed and heating the samples. Figure 7.6 shows a schematic of how laser trapping works, the 1064nm light is tightly focused using the NA=1.3 oil immersion objective (Nikon plan fluorite). The suspended diamond particles suspended in DI water an aqueous solution are then trapped at the beam waist of the focussed beam.

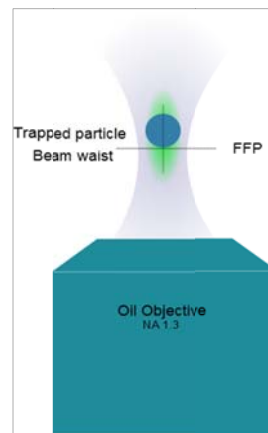


Figure 7.6: The schematic diagram of trapped and suspended diamond particles in the beam waist.

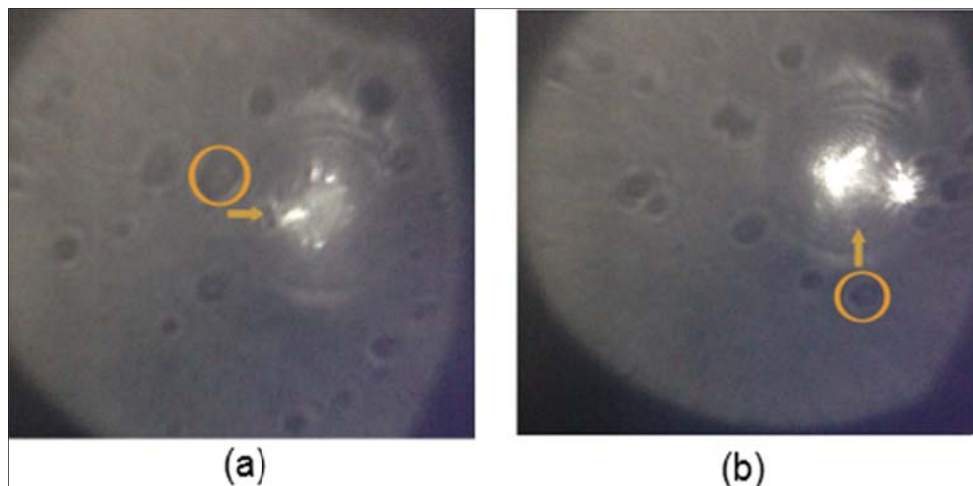


Figure 7.7: The captured images of manually moving the suspended diamond particles in the X, Y axes towards the focus of the 532 nm laser on the sample. Image 7.7 (a) the diamond particle is moving to the right along the x – axis towards the focus point and in the image of 7.7 (b) the diamond particle is moving upwards along the Y – axis towards the focus point.

The power of trapping laser plays a vitally important role in the trapping process of the particles and is highly dependent upon the size of particles. Trapping of particles is only possible when



they are in high intensity field. During trapping the particles are stabilised by balancing the gradient  $F_{Scat} = Q_{Scat} \frac{n_m P}{c}$  and scattering  $F_{grad} = Q_{grad} \frac{n_m P}{c}$  forces that act on the particle in different directions; the scattering force acts on the nano particles in the direction of radiation, whereas the gradient force is caused by the reflection of the beam from the surface of nano particle and thus acts in the opposite direction of radiation. So, the total trapping force on a suspended diamond particle in specimen is given by

$$F_{Tot} = Q_{max} \frac{n_m P}{c}$$

Where  $Q_{max}$  is the maximum value of trapping quality factor ( $Q_{max} = Q_{scat} + Q_{grad}$ ). It is therefore possible to move the trapped diamond particles by moving the laser light in the axial and transverse directions.

Table 7: Calculated values of the beam waist, radius and trapping volume of laser

( $\lambda$ ) nm	NA	Beam Waist ( $w_o = \frac{n\lambda}{\pi NA}$ ) $\mu\text{m}$	Beam radius ( $r = \frac{w_o}{2}$ ) $\mu\text{m}$	Rayleigh range $R_r = \frac{\pi w_o^2}{\lambda}$ $\mu\text{m}$	Trapping Volume ( $v = \frac{n^4 \lambda^3}{4\pi^2 NA^4}$ ) $\mu\text{m}^3$
	0.9	285	-		-
532	1.3	197	-		-
	1.4	183	-		-
	0.9	368	-		-
687	1.3	255	-		-
	1.4	237	-		-
	0.9	570	285	0.95	0.250
1064	1.3	395	197.5	0.46	0.056
	1.4	367	183.5	0.397	0.042

The trapping of suspended diamond particle is only possible when they are in high intensity field. Figure 7.7 (a) image showing the movement of diamond particle towards the focus point while moving along the x – axis. The NV color centers in diamond particles start to glow at focus point of 532nm laser. The same process can carried out while moving the particle upwards towards the focus point the images in figure 7.7 (b) showing the movement of the particle by using the piezo-system.

Figure 7.8 shows the results of moving trapped diamond particles along the x and y direction. The movement of trapped particles was achieved by carefully moving the whole sample using the piezo-motor system. The trapped particle at the central of the beam waist appeared stable and drifts free during movement. The particle was moved up to  $5\mu\text{m}$  in the y axis and  $2\text{-}3\mu\text{m}$  in x axis direction. The power of trapping laser varies for different particle size and power required to trap depends solely on the size and symmetry of diamond particle at focus of beam waist. The figure 7.8 showing the results of trapped suspended diamond particle and these diamonds particles move along in the x, y direction.

The movement of trapped particles can be control by carefully moving the sample holder mounting on the piezo-system. The trapped particle moved in x, y direction by moving the sample holder with smallest possible step of piezo-system.

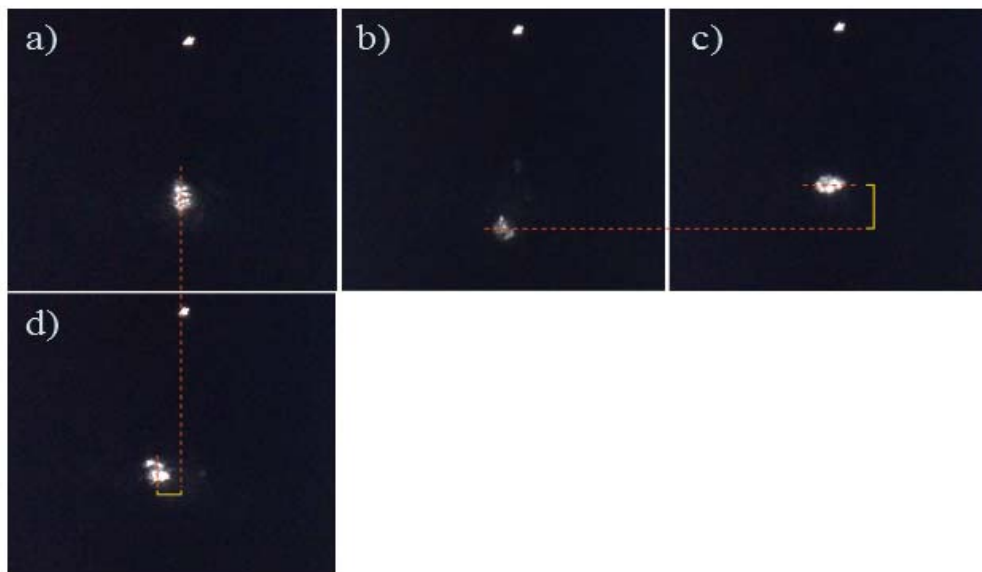


Figure 7.8: The captured images of the trapped and suspended diamond particles at the focus of the 532 nm and 1.064  $\mu\text{m}$  laser upon the sample. Images 7.8 (a) and (d) show the diamond particle moving along the X – axis. Images 7.8 (b) and (c) show when the diamond particle is moving to the upward along Y – axis.

The trapped particle at the central of the beam waist appeared stable and drift free particle. During the experiment, the movement of trapped particle was performed in micrometer scale to avoid entrapping of particle for large distance. The particle can move 5  $\mu\text{m}$  distances during the y axis movement and 3  $\mu\text{m}$  in x axis direction. Particles were trapped using 8.4mW power from the 1064nm laser source and about 20 – 30 $\mu\text{W}$  of 532nm excitation (which is equal to the 0.02 pN total optical force exerts on dielectric particle for trapping). The images showed in figure (7.8) were obtained using the CCD camera before and after the movement of the trapped particle. The position of the z axis piezo-system is maintained at 52.1 $\mu\text{m}$  to obtain the good focus of laser on the sample for trapping.

## **7.5 Future work**

### **7.5.1 NMR Imaging**

NMR imaging can be used to image the internal works of live specimens, by using an external magnetic field. The detail of the specimen structure is captured in the form of an image by using an external magnetic field. The specimen structure is comprised of tissues and each tissue contains water molecules. A single water molecule is a combination of oxygen, two hydrogen atoms. The external magnetic field causes water molecules in the specimen to align in the direction of applied field. A non-uniform magnetic field is then applied and the change in molecule alignment used to image the structure of the specimen.

The confocal microscope setup shown in figure 6.1 can also serve as an ideal setup for obtaining the NMR images of living specimen. The existing microscope setup would simply be upgraded by inserting an electro-magnet around the sample space to allow a magnetic field to be applied. The gradient and the amount of applied external magnetic field is control by the amount of applied voltage to the electromagnetic. NMR imaging offers a way to image a specimen without any hazards of affecting the tissue of specimen as compare to the x ray,  $\gamma$  ray imaging [64].

### **7.5.2 Optical Properties of Various QDs**

In 1980 Alexei Ekimov and Louis E. Brus demonstrated quantum dots in a glass matrix and also in a colloidal solution respectively [65]. Quantum dots are semiconductors crystallite nano-

particle with a diameter of size smaller than the exact Bohr radius. These nano-particles have the ability to exhibit the quantum mechanical properties of the confined system. The size and the material of assembled QDs play a key role for the determination of absorbed and shifted wavelength of light.

The setup of microscope was equipped with two excitation laser wavelength which makes this setup suitable for studying the optical properties of different QDs. Optical properties character behavior of QDs can be analyzed whose prepared with material have absorption wavelength range 400 nm – 700nm. QDs are highly promising candidates for biomedical imaging, drug delivery, photovoltaic devices, biosensors and for quantum computation. And hence this newly developed dual-beam microscope system should provide an ideal tool for studying these dots and their applications.

## Bibliography:

- [1] D. F. Walls 'Evidence for the quantum nature of light', *Nature* Vol. 280, 9 August 1979.
- [2] R. Hanbury Brown, R. Q. Twiss 'Correlation between photon in two coherent beams of light', *Nature* Vol.177, 27 – 29, 07 January 1956
- [3] Ashkin, A., 'Acceleration and trapping of particles by radiation pressure', *Phys. Rev. Lett.*24, 156 (1970)
- [4] Hopkins, R.J. Symes, R. Sayer, R.M. Reid, 'Determination of the size and composition of multicomponent ethanol/water droplets by cavity-enhanced Raman scattering', *Chem Phys. Lett.* 380, 665 (2003)
- [5] S. W. Hell, J. Wichmann, 'Breaking the diffraction resolution limit by stimulated emission' *Optics Letter*, Vol. 19, No. 11, June 1, 1994.
- [6] E. Raymond Andrew, 'NMR Imaging ' *Acc. Chem. Res.* 16, 114 – 122, 1983.
- [7] C. Kurtsiefer, S. Mayer, P. Zarda and H. Weinfurter, 'Stable solid state source of single photons', *Phys Rev. Lett.* , Vol 85, 290 – 293, 2000.
- [8] A. Kuhn, M. Hennrich and G. Rempe, 'Deterministic single photon source for distributed quantum networking', *Phys. Rev. Lett.* , Vol. 89, 067901, 2002.
- [9] C. Keir, Neuamn, M. Steven, 'Optical trapping', *Rev. Sci. Instrum.*, Vol. 75, No. 9, 2787 -2810, 2004.
- [10] J. Matthew Lang, M. Steven, 'Laser based optical tweezers', *Am. J. Phys.* 71(3), March 2003.
- [11] A. Beveratos, S. Kuhn, R. Brouri, T. Gacoin, P. Grangier. 'Room temperature stable single photon source', *Eur. Phys. J. D* 18, 191 – 196, 2002.
- [12] Marcus W. Doherty, Neil B. Manson, P. Delaney, F. Jelezko, J. Wrachtrup. 'The nitrogen vacancy colour center in diamond', *Phys. Rep.* Vol. 528, Issue 1, P. 1 – 45, 2013.
- [13] J. C. Maxwell, 'A treatise on electricity and magnetism', Vol. 1, Oxford: Clarendon Press, 1873
- [14] P. Lebedev, 'Analysis of pressure forces of light' *Ann. Physic* 311, 433 – 458, 1901(5r2).
- [15] D. Preece, 'Novel uses of spatial light modulators in optical tweezers', PhD thesis. Department of Physics and Astronomy, University of Glasgow, Scotland, 2011
- [16] Martin Persson, 'Advances in holographic optical trapping' PhD thesis, Department of physics, University of Gothenburg, Sweden, 2013
- [17] M. Fox, 'Quantum Optics – An introduction', Oxford University Press, Published 2006.

- [18] Francesco Pampaloni, 'Force sensing and surface analysis with optically trapped microprobes', PhD thesis, Faculty of Natural Science IV, Chemical and pharmaceutical industry, University of Regensburg, Germany, 2002.
- [19] Book title, 'Handbook of molecular force spectroscopy' Aleksandr Noy, 30 – 31, ISBN – 13: 978 – 0 – 387 – 49989 – 5, Springer Science, 2008
- [21] J. Molly, M. Padgett, 'Lights, action: optical tweezers', *Contemporary Physics* 43, 2787- 2809, 2004
- [22] K. Svoboda, S. M. Block, 'Biological application of optical forces', *Annual Review of Biophysics and Biomolecular Structure* 23, 247 – 285, 1994
- [23] E. Fällman, O. Axner, 'Design for fully steerable dual trap optical tweezers', *Appl. Opt.* 36, 2107 – 2113, 1997
- [24] K. Visscher, G. J. Brakenhoff, J. J. Krol, 'Micromanipulation by multiple optical traps created by a single fast scanning trap integrated with the bilateral confocal scanning laser microscope', *Cytometry* 14, 105 – 114, 1993
- [25] Serway, Raymond A, 'Physics for Scientists & Engineers', 3rd ed. Published (1990). P.1150. ISBN 0-03-030258-7
- [26] R. L. Pfleeger, L. Mandel. 'Interference of independent photon beams', *Phys. Rev.* Vol. 159, Issue 5. pp. 1084 – 1088. 1967.
- [27] M. H Mahran, M. Venkata Satyanarayana, 'Bunching and antibunching properties of various coherent states of the radiation field', *Phys. Rev. A* 34, 640 – 643, 1986.
- [20] Andrew D. Greentree, Barbara A. Fairchild, Faruque M. Hossain and Steve prawer, 'Diamond integrated quantum photonics', *Mate. Today*, Vol. 11, Num. 08, September 2008.
- [21] X. Luo, Z. Liu, Bo Xu, Dongli Yu, Y. Tian, H. T. Wang and Julong He, 'Compressive strength of diamond from first – principle calculation', *J. Phys. Chem. C* 2010, 114, 17851 – 17853.
- [22] S. Tong Lee, Z. Lin, Xin Jiang 'CVD diamond films: nucleation and growth', *Mater. Sci. Eng.*, 25 (1999), 123 – 154.
- [21] R. C. Burns, J. O. Hansen, R. A. Spits, M. Sibanda, C. M. Welbourn, D. L. Welch, 'Growth of high purity large synthetic diamond crystals', *Diamond Ralet. Mater.* 8 (1999), 1433 – 1437
- [23] Images of diamond took from 'Glittering Stones collection' [www.glitteringstones.com](http://www.glitteringstones.com)
- [24] R. C. Burns, in: S. Saito, O. Fukunaga, M. Yoshikawa (Eds), 'Science and Technology of New Diamond', KTK Scientific Publishers/Terra Scientific Publishing Company, Tokyo, 1990, pp. 197 – 201.
- [25] M. Akaishi, H. Kanda, S. Yamaok, 'Synthesis of diamond from graphite – carbonate systems under very high temperature and pressure', *J. Cryst. Growth*, 104, 578 – 581, 1990

- [26] Y. V. Babich, B. N. Feigelson, A. P. Yelisseyev, 'Nitrogen aggregation and linear growth rate in HPHT synthetic diamonds', *Diamond Relat. Mater.*, Vol. 13, 1802 – 1806, 2004
- [27] J. Isberg, J. Hammerberg, E. Johansson, T. Wilkström, D. J. Twitchen, A. J. Whitehead, S. E. Coe, G. A. Scarsbrook, 'High carrier mobility in single – crystal plasma deposited diamond', *Science* 297, 1670 (2002).
- [28] M. H Nazare, A. J Neves, 'Properties, growth and application of diamond', INSPEC Publisher
- [29] R. Mildren, J. Rabeau, 'Optical engineering of diamond', Publisher WILEY – VCH . 2013
- [30] Bundy, F. B., Hall, H. T., Strong, H. M., Wentorf Jr., R. H., *Nature* 176, 51 – 55, 1955
- [31] Bundy, F. P., *J. Chem. Phys.* 38, 631 – 643, 1963
- [32] May, P. W.: *Philos. Trans. R. Soc. Lond. A* 358, 473 – 495, 2000
- [33] J. J Gracio, Q. H. Fan, J. C. Madaleno, 'Diamond growth by chemical vapour deposition', *J. Phys. D: Appl. Phys.* 43, 3740 17, 2010
- [34] K. Febisiak, E. Staryga, 'CVD diamond from growth to application', *J. Achieve. Mater. and Manuf. Engin.*, Vol 37, Iss 02, December 2009
- [35] P. Calvani, A. Corsaro, F. Sinisi, M. C. Rossi, G. Conte, E. Giovine, W. Ciccognani, E. Limiti., *Microw. Opt. Technol. Lett.*, 51, 2786, 2009
- [36] Y. Gurbuz, P. W. Kang, J. L. David, Jr. J. A. Kerns, Q. Zhou, 2005 *IEEE Trans. Power Electron.* 201.
- [37] Pang L. Y. S., Chan S. S. M., Johnston, Chalker P. R., Jackman R. B., 1997, *Diamond Relat. Mater.* 6 333.
- [38] C. A. Foell, A. M. Zagoskin, J. F. Young, 'Engineering Silicon Based Photonic Crystal Cavities for NV – center Quantum Information Processing', *Optical and Spectroscopy*, Vol. 108, No. 2, pp. 225 – 229, 2010
- [39] B. Grotz, M. V. Hauf, M. Dankerl, B. Naydenov, S. Pezzagna, J. Meijer, F. Jelezko, M. Stutsmann, J. Wrachtrup, F. Reinhard, J. A. Garrido, 'Charge state manipulation of qubit in diamond', *Natur. Commun.*, 3:729, DOI: 10.1038/ncomms1729, 06 March 2012
- [40] Walter A. Harrison, 'Elementary Electronics Structure', World Scientific Publication Co., p. 435, 1999
- [41] [http://wwwee.ccnycunyu.edu/www/web/crouse/EE339/Lectures/Bravais\\_Lattice.htm](http://wwwee.ccnycunyu.edu/www/web/crouse/EE339/Lectures/Bravais_Lattice.htm) , Source of figure (4.1) on page 29
- [42] [http://en.wikipedia.org/wiki/Diamond\\_cubic](http://en.wikipedia.org/wiki/Diamond_cubic) , Source of figure (4.2) on page 30.
- [43] Dingwei Zheng, 'Study and Manipulation of Photoluminescent NV color center in diamond', Phd thesis. 27 Oct. 2010

- [44] <http://en.wikipedia.org/wiki/Phonon>.
- [45] Per Nilsson, 'Single photon sources using the confocal microscope', Master thesis. 7<sup>th</sup> Nov. 2009.
- [46] Viva R. Horowitz, Benjamin J. Aleman, D. J. Christle, A. N. Cleland, D. A. Awschalow, 'Electron spin resonance of nitrogen vacancy centers in optically trapped nanodiamonds' PNAS, 109(34): 13493 – 13497, 2012.
- [47] A. Cuche, A. Drezet, J. Francois Roch, Francois Treussart, Serge Hunat, 'Grafting fluorescent nanodiamonds onto optical tips' , J. Nanophotonics, Vol. 4, 043506, 9<sup>th</sup> March 2010.
- [48] B. I. Kharisov, Oxana V. Kharisov, L. Chavez Guerrero, 'Synthesis techniques, properties and application of nanodiamonds', Taylor & Francis Co., 40:2, 84 – 101, 16 Feb. 2010.
- [49] M. Minsky, U.S. Patent 3013467, 'Microscopy Apparatus' , Dec. 19, 1961 (Filed Nov. 7, 1957)
- [50] M. Minsky, 'Memoir on inventing the confocal scanning microscopy', Scanning, 10 (1988) 128
- [51] W. Lukosz, M. Marchand. 'Optica Acta', 10 (1963) 241
- [52] M. D. Egger, M. Petran. Science, 157 (1967) 305
- [53] M. Petran, M. Hadravsky, M. D. Egger, R. Calambos, J. Opt. Soc. Am., 58 (1968) 661
- [54] Barry J. Elliott, M. Gilmore 'Fiber Optic Cabling' 2<sup>nd</sup> Edition, Pg. 70, 2002, ISBN 0 7506 5013 3.
- [55] E. Raymond Andrew, 'NMR Imaging 'Acc. Chem. Res. 16, 114 – 122, 1983
- [57] A. I. Ekimov, A. A. Onushchenko, 'Quantum size effect in three dimensional microscope semiconductor crystals' JETP Lett. Vol. 34, Issue 6, pp. 345 – 349, 1981



